SPATIALLY RESOLVED SPECIES AND TEMPERATURE PROFILES IN THE OXIDATIVE DEHYDROGENATION OF ETHANE ON MONO AND BIMETALLIC CATALYSTS AT SHORT CONTACT TIMES

A THESIS

SUBMITTED TO THE FACULTY OF THE GRADUATE SCHOOL

OF THE UNIVERSITY OF MINNESOTA

BY

DAVID NYASHA NARE

IN PARTIAL FULFILLMENT OF THE REQUIREMENTS

FOR THE DEGREE OF

MASTER OF SCIENCE

LANNY D. SCHMIDT, ADVISOR

JANUARY 2010

Acknowledgements

I would like to thank Professor Schmidt for giving me an opportunity to join his research group. His guidance and insight have helped me further challenge myself and better understand the world of science and engineering in a broader sense.

My pursuit of graduate studies would not have been possible without the motivation of teachers I have had in high school at St. Mary's Magdalene's, during Advanced Level studies at Marist Brothers Nyanga and finally during my undergraduate program at New Jersey Institute of Technology. Dr. Kabba, a friend of my father's who worked for Merck, essentially introduced and inspired me to chemical engineering, a field I have grown to love immensely.

I also would like to thank Dr. Anders Bitsch-Larsen for establishing me with the catalytic partial oxidation processes. Many thanks to Brian Michael for introducing me to the spatial profiles technique, for the many discussions we have had, and with whom part of this work is collaborated with. I also extend my thanks to visiting scientist Dr. Alessandro Donazzi for helping me during my first few weeks in the lab. I also extend my highest gratitude to Jushua Colby and Mark Huberty for proofreading this thesis under a tight timeframe.

Furthermore, the entire Schmidt group has been very supportive throughout the many conversations and group presentations we have had. Finally, I am grateful for the unwavering support my family has given me in all aspects of life and for allowing me to study far from home. I thank my parents for keeping up with me in my search and pursuit of excellence throughout my academic career. Their unconditional love, support and inspiration drives me every day.

Dedication

This work is dedicated to my beloved grandmother Merina, who reared me from childhood until my late teenage years, to my dad Bakela, for teaching me to love and have a passion for science and to my mom Lydia, for always putting things in perspective and recognizing the big picture.

To my younger brothers Lester and Thabo, with hope that I have set an example for them, and that they shall recognize their talents, so as excel above and beyond borders they thought impenetrable.

Abstract

The oxidative dehydrogenation of C_2H_6 to C_2H_4 was studied on monometallic and bimetallic 45 PPI foam monoliths at ~8ms contact time. The capillary sampling method was used to measure concentration and temperature profiles along the reactor. Pt and Rh showed quite different product distributions; Rh was highly selective to syngas formation (~80%), whereas Pt produced high selectivity to non-equilibrium C_2H_4 (~55%). Spatially profiles show that Rh oxidizes feed C_2H_6 rapidly in the first 3mm of the catalyst to produce H_2O, CO and H_2 with >99% O_2 conversion, followed by endothermic steam reforming, producing more syngas. Pt consumes O_2 slower than Rh, with incomplete conversion at all tests. However, Pt shows poor endothermic reforming activity, hence is able to sustain high reactor temperatures, increasing C_2H_6 dehydrogenation rates. H_2 addition tests show a two zone model; preferential oxidation to H_2 raising the catalyst temperature while preserving C_2H_6, followed by C_2H_4 production. On Rh, H_2 addition produced minimal change. The differences in catalytic performances are attributed to the high reforming and oxidation capability of Rh compared to that of Pt.

The effect of Sn and Cu addition to Pt was also studied. Results show that bimetallic catalysts exhibit higher C_2H_6 and O_2 conversion and selectivity to C_2H_4 than Pt. On Pt, production of C_2H_4 occurs further into the monolith with increase in C/O. In contrast, bimetallic catalysts show C_2H_4 production almost instantly, particularly because the temperatures would have exceeded 750^oC (when homogeneous ignition of C_2H_6 occurs) closer to the front face. Pt-Sn and Pt-Cu showed that they are superior to Pt in terms of deep oxidation of H_2, with higher selectivity to C_2H_4 (85%). Pt-Sn and Pt-Cu are superior due to improved oxidation rates resulting in attainment of homogenous ignition temperatures earlier into the monolith C_2H_6 conversion rates. All catalyst show equally poor reforming ability, an attribute desirable in sustaining reactor temperatures, thereby obtaining high selectivity to C_2H_4.

In summary, chapter 1 discusses motivation for research, background on CPO reactors and introduces the capillary sampling technique. Chapter 2 details experimental methods used. Chapter 3 focuses on ODH on Pt and Rh, while chapter 4 discusses ODH on Pt, Pt-Sn and Pt-Cu. Finally, chapter 5 concludes with future directions.

Table of Contents

List of Figures

List of Tables

Definitions and Abbreviations

Carbon to Oxygen Ratio (C/O)

It is the ratio of the amount of atomic carbon in the feed to that of atomic oxygen in the feed. C/O =1 means oxygen rich and C/O =2 means fuel rich.

$$C/O = \frac{amount\ of\ \ atomic\ carbon\ in\ feed}{amount\ of\ \ atomic\ oxygen\ in\ feed}$$

Conversion (X)

It refers to the difference between the inlet and outlet of species *i* as a ratio of the inlet.

$$X = \frac{N_i^{in} - N_i^{out}}{N_i^{in}}$$

Where N_i^{in} and N_i^{out} refers to number of inlet and outlet moles for species *i* respectively.

Selectivity to H (S_H)

It refers to the fraction of element H that is in a reactant and has been reported to the particular product. Only the converted fuel is considered.

$$S_H = \frac{\alpha_i N_i}{\alpha_{fuel}(N_{fuel}^{in} - N_{fuel}^{out})}$$

Where α_i is the number of H's in *i* and N_i is the number of moles of product *i*.

Selectivity to C (S_C)

Similar to selectivity in H, It refers to the fraction of element C that is in a reactant and has been reported to the particular product. Only the converted fuel is considered.

$$S_c = \frac{\beta_i N_i}{\beta_{fuel}(N_{fuel}^{in} - N_{fuel}^{out})}$$

Where β_i is the number of C's in *i* and N_i is the number of moles of product *i*.

Yield (Y)

It is defined as the ratio of the amount of product i formed to the ratio of the reactant feed for the limiting component. For ethane CPO, the limiting component is always fuel.

$$Y_i = \frac{\alpha_i N_i}{\alpha_{fuel} N_{fuel}^{in}}$$

Alternatively, one it can also be defined as fuel conversion multiplied by selectivity.

ODH

Oxidative Dehydrogenation

CPO

Catalytic Partial Oxidation

SLPM

Standard Liters per Minute

SCCM

Standard Cubic Centimeters per Minute

FHS

Front Heat Shield (non catalytic portion of catalyst located in the front of the catalyst)

BHS

Back Heat Shield (non catalytic portion of catalyst located in the back end of the catalyst)

QMS

Quadrupole Mass Spectrometer

GC

Gas Chromatograph

Chapter 1

Introduction

1.1 Summary

This chapter begins by briefly discussing the energy problem as it relates to the motivation of this work. The importance of ethylene to the chemical industry and its conventional production method (steam cracking) are then described. Due to the numerous disadvantages that lie with steam cracking, the concept of catalytic partial oxidation at short contact times is presented, covering concepts such as the production of synthesis gas, olefins and oxygenates. A literature review of the catalytic partial oxidation of ethane follows, where comparable performance to steam cracking in terms of conversion and selectivity were obtained. However, the literature fails to describe the mechanism by which catalytic partial oxidation. Some attempts to arrive at mechanism as proposed by various research groups are presented. Noting that product evolution inside the catalyst will add valuable data to modeling and experimental efforts, the concept of spatially resolved measurements is introduced as it applies to how species and temperature profiles were obtained.

1.2 Research Motivation

The late Nobel laureate Professor Richard Smalley presented "The Top Ten Problems for Humanity for Next 50 Years" at a conference in 2003, by order of priority, as energy, water, food and environment, only to mention a few [1]. As far as national government spending has been concerned, arguably the top two challenges ahead of us are energy and the environment. Given this state of the union, multilateral, intercontinental and collaborative governments' efforts are needed to not only provide tools to create alternative forms of energy, but to also improve existing processes. These processes range from how energy is currently harnessed, greenhouse gas emissions control, low cost chemicals as well as mitigation of chemical and biochemical waste among others.

Currently, the annual global population growth rate is estimated at 1.17% [2], meaning the world population may exceed 9 billion by the year 2040. Such a remarkable growth poses challenges to the human race and the environment alike; increase in demand for food, decrease in conventional fuel resources which are non-renewable, large increases in energy consumption and negative impact on land and marine life. The strain of these resources is further exacerbated by terrorism, economic and political factors. Crude oil still remains the top source of energy for transportation and chemicals in the world. A trend of its historical price hikes is shown below, topping at $140 a barrel last year.

Figure 1- 1: World trends in crude oil prices.

Because crude oil is a raw material in many processes, its prices drive chemical and transportation costs as well as influencing products that rely on it as a raw material. For this work, the chemical ethylene is the focus; its importance to the chemical industry is explored, and efforts to find an alternative means of production are presented as they relate to this thesis, all as part of an effort to combat a much wider global problem.

1.3 The Importance of Ethylene

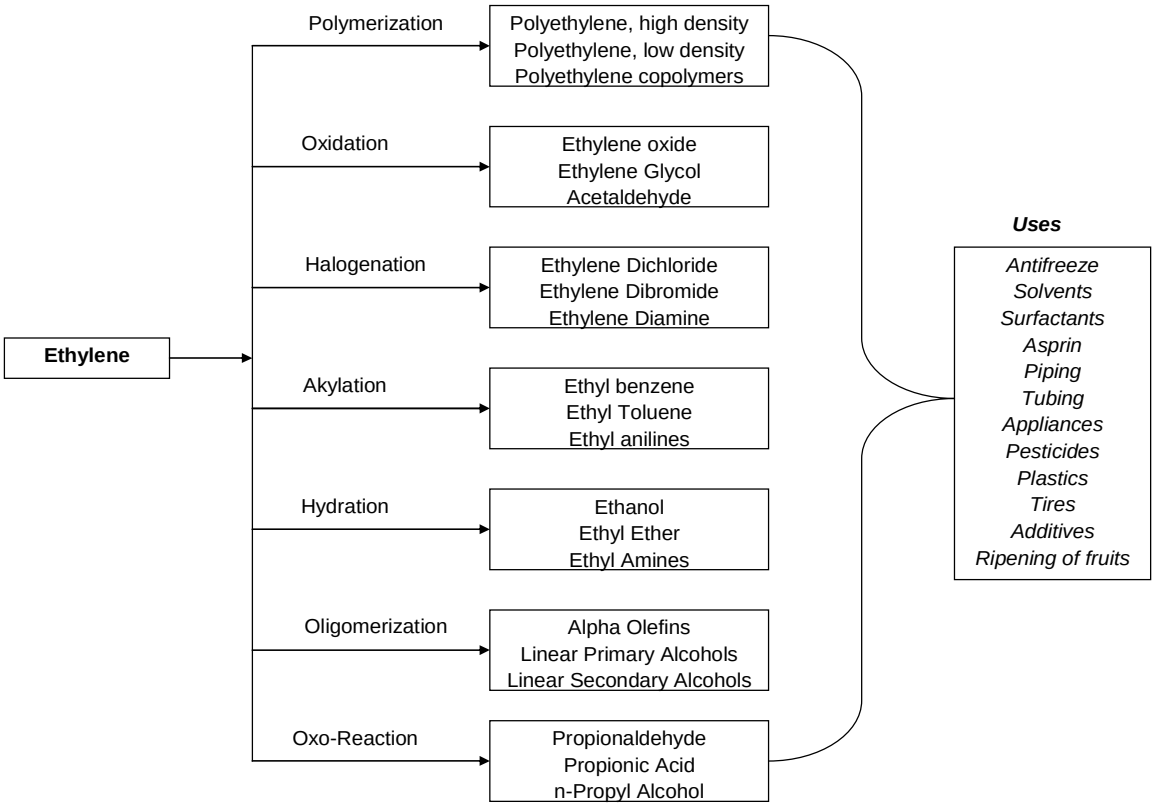

Figure 1- 2: Commercially important reactions of ethylene.

Ethylene, also known as ethene ($H_2C=CH_2$), is considered a highly reactive compound due to its double bond. It can be converted into a multitude of intermediate and end products on large industrial scale as seen in Figure 1-2. Ethylene, alongside

species containing 2-4 carbons, is classified as a light olefin, whose production growth rate is expected to remain above world GDP growth rates [3]. The current world production of ethylene is estimated to be over 110 million tons/year, making it the single most basic and important building block in the petrochemical industry [4, 5]. To illustrate its versatility, the commercially important chemical reactions of ethylene are organized top down into seven 7 basic reaction groups according to their chemistry in Figure 1-2. While the list is not exhaustive, it gives insight as to why ethylene is indeed a keystone to the petrochemical industry. As such, in recent times, industry and academic institutions have tackled the growing need to utilize technologies that favor higher ethylene production in line with its demand, cost and use.

1.4 Conventional Ethylene Production via Steam Cracking

Ethylene is currently produced almost exclusively from ethane, propane, heavy paraffins, virgin crude oil naphtha fractions, kerosene and gas oil. The total feedstock is estimated to be 300 [6] and 85 [3] million tons for world and U.S production respectively. For U.S production, 55 million tons of the feedstock comes from ethane derived from natural gas, while 15 million tons is propane feed also from natural gas. The majority of the remaining feedstock for U.S production comes from naphtha (containing 4-7 carbons) derived from crude oil.

To understand why the U.S prefers to use ethane and propane to produce ethylene, factors that determine feedstock for any chemical process have to be considered. Generally these include reaction conditions, complexity of processing unit, feedstock availability, price as well as capital requirements [5]. Natural gas has been the basis for the U.S energy industry for the past half century, therefore it has been attractive to separate and sell natural gas liquids [7]. Whereas in Europe, the feedstock is more than 90% [5] naphtha because of the unavailability of liquefied petroleum gases and the demand for heavier gas oils as heating fuels.

The production of ethylene is primarily by steam cracking [8]. For an ethane feed, the steam cracking reaction occurs as follows:

$$C_2H_6 \xrightarrow[heat]{steam} C_2H_4 + H_2 \qquad \Delta H^o = +136 \text{ kJ/mol} \qquad (1.1)$$

A steam cracker employs extreme temperature ranging from 850^{o}C from the outlet of the furnace to -165^{0}C in the cryogenic hydrogen-methane separation. The fuel and steam are fed into heated tubes where thermal decomposition reactions occur at high temperatures, a process known as pyrolysis. These extreme temperatures require introduction of numerous construction material including carbon steel, high chrome-nickel alloys for the pyrolysis tubes, aluminum in the cryogenic systems and molybdenum alloy for the methanator (which is exposed to high hydrogen partial pressures at elevated temperatures) [7].

Steam crackers have several disadvantages. The process is energy intensive from the endothermic chemistry of steam reforming. It is considered the most energy consuming process in the chemical industry, where it globally uses approximately 8% [9] of the sector's primary energy use (excluding the energy content of final products). Large furnaces and fired heaters have to be built to provide the large amounts of energy required. Steam is added to the feedstock to reduce the partial pressure of the hydrocarbons in the coil [7]. It does so by reducing the carbon formation that clogs tubes causing significant pressure drops. In the pyrolysis reactor, reactions occur mostly by free radical mechanisms, a process that involves complex simultaneous reactions. In one simplified pathway, steam cracking can be thought to proceed via consecutive dehydrogenation steps as follows:

$$C_2H_6 \xrightarrow{-H_2} C_2H_4 \xrightarrow{-H_2} C_2H_2 \xrightarrow{-H_2} 2C \qquad (1.2)$$

This process produces significant amounts of unconverted carbon (coke) and certain equipment, notably the pyrolysis furnaces and dehydrogenation reactors, have to be periodically shutdown to allow for regeneration through controlled combustion. The operational steps are potentially hazardous to the designer and operator alike, as ethylene plants tend to have significant inventory levels of light hydrocarbons at elevated pressures. The same phenomenon affects heat exchangers, which are prone to fouling. Fouling is a complex science and is still an unresolved problem in the process industry.

Simply stated, it is the degradation in heat transfer or increase in thermal resistance due to buildup of polymers or coke on the heat transfer surface. Because of increased thermal resistance, higher energy inputs are required [10]. Additionally, the long residence time in a typical steam cracker, which is on the order of 1 sec, also contributes heavily to the coking process [8].

Ethane conversion in a steam cracker is about 65-70% and >10% of the feed is recycled for heating the pyrolysis furnace [11]. NO_x emissions from flames in the furnace are then produced, in addition to an estimated 180-200 [4] million tones of CO_2 emissions worldwide. Reduction of these emissions can help meet the standards set forth by the Kyoto Protocol [12]. Not only is the efficiency and reliability of steam cracking dependent on performance, there are a greater number of support systems which generally require an investment on the order of 40-70% [7] of the cost of process facilities. A typical ethylene plant contains over 400 pieces of equipment ranging from fired heaters, drums, compressors and fractionation towers to pumps.

Despite the disadvantages noted with steam cracking, it is still widely used in industry because of the unmatched yield. However, rising costs for raw materials and ever increasing competition have made margins in ethylene production quite slim in recent years. Therefore, from environmental, process performance, economic and safety perspectives, it is of interest to improve the in efficiency and mitigation of emissions from steam cracking. More importantly however is reactor performance. The pyrolysis section (reactor) is considered the heart of an ethylene plant [7] as it produces all the products of the plant, while others serve as separation and purification units. For this reason, the pyrolysis section represents the greatest potential for improvement in feedstock utilization, thermal efficiency and ethylene productivity, a focus for this work.

1.5 Background on Catalytic Partial Oxidation at Short Contact Times

In 1993, Hickman and Schmidt did experiments which produced >90% selectivity to carbon monoxide (CO) and hydrogen (H_2) with almost complete conversion of methane (CH_4) at reaction conditions with 10 ms residence times [13]. The results contributed heavily to the catalytic community since the process of converting abundant resources such as natural gas to valuable fuels and chemicals in remote locations amid rising fuel prices posed numerous possibilities. The technique, termed Catalytic Partial Oxidation (CPO) as demonstrated by Hickman and Schmidt, had been known since 1929. The CPO process uses a catalyst metal, e.g Pt, Rh deposited on a support (typically alumina), where 50% of stoichiometric combustion oxygen (O_2) is introduced. For methane CPO, the reaction proceeds as such:

$$CH_4 + \frac{1}{2}O_2 \rightarrow CO + 2H_2 \qquad \Delta H^o = -38 \text{ kJ/mol} \qquad (1.3)$$

For the last 15 years, the Schmidt group has developed CPO reactors for liquid, solid and gas feeds, maximizing on the benefits of CPO. Partial oxidation reactions are exothermic; hence no external source of heating is required. The heat produced is enough to sustain the reaction until normal shutdown, making them autothermal [13]. By virtue of millisecond contact time, the reactions can be carried out in much smaller reactors, therefore tunable. Parameters such as flow rate, pressure, catalyst composition and geometry, and fuel to oxygen ratios only to mention a few, can be effectively changed and different ratios used to tailor products unlike conventional reactors. Consequently, numerous attempts to understand the applicability of CPO reactors for many processes have been made in the last decade. CPO has been used in the partial oxidation to synthesis gas, oxygenates and to valuable chemicals and fuels as will be discussed next.

1.5.1 CPO to Syngas

Generation of synthesis gas (syngas, CO and H_2) is very attractive for mobile applications because synthesis gas can be used to generate electricity in solid oxide fuel cells and to abate pollutants in internal combustion engines [14]. In addition, on board reforming of these liquid fuels in return eliminate gaseous H_2 storage issues and eliminates the need for very dangerous H_2 gas stations. Syngas is also used for the production of chemicals and fertilizers [15]. As such, the Schmidt group has investigated using CPO to generate high selectivities to syngas.

Subramanian et al took model hydrocarbon mixtures (*n*-octane + *i*-octane, *n*-decane + *n*-hexadecane, *n*-decane + *n*aphthalene) into a CPO reactor over Rh coated monoliths to try and mimic gasoline and diesel fuels. They were able to get selectivities to syngas exceeding 70%, demonstrating the ability of CPO to oxidize hydrocarbon mixtures, including hydrogen-deficient poly-aromatic compounds without deterioration in reactor performance [16]. Along the same line of higher hydrocarons, Krummenacher et al were able to perform catalytic partial oxidation of *n*-decane and *n*-hexadecane over Rh monoliths producing syngas selectivities >80% at >99% fuel conversion. These hydrocarbons (with high boiling points) were introduced to the reactor as vaporized liquids using an automotive fuel injector. CPO of low sulfur diesel fuel was also carried out, producing syngas at >98% fuel conversion for several hours of stable operation [17].

Autothermal reforming (ATR), which combines CPO and steam reforming (SR) [18], can also be used to produce renewable hydrogen from ethanol as illustrated by Deluga et al. Ethanol and ethanol water mixtures were converted into H_2 with 100% selectivity and >95% conversion over rhodium-ceria (Rh-Ce) catalyst at 10 ms residence time [19]. Here again, CPO proves potential for low cost H_2 for portable applications.

Recently in the Schmidt group, conversion of biopolymers to synthesis gas was done by Colby et al, where the commonly biomass-to-liquids process (BTL) was integrated into a single autothermal catalytic reactor producing 80% hydrogen selectivity at a H_2/CO ratio =2.3 [20]. A syngas ratio of 2 is highly desirable in Fischer-Tropsh processes where syngas can be converted to methanol, dimethyl ether and synthetic diesel fuel. Salge et al also demonstrated high syngas yields when droplets of nonvolatile fuels

such as soy oil and glucose-water solutions were introduced into a CPO reactor, a technique termed reactive flash volatilization [15].

1.5.2 CPO to Oxygenates

By increasing the carbon length and increasing the fuel to oxygen ratio, one can produce high yields to oxygenated compounds. The current production of these oxygenates requires multiple stages, expensive catalysts, large residence times and careful temperature control [21].

Iorganoglou and Schmidt partially oxidized *n*-butane over a single layer of Pt-10% Rh gauze at atmospheric pressure in a rich fuel regime at 2-10 ms contact time. They showed that an optimum regime existed, where the space velocity could be tailored to maximize oxygenate production reaching as high as 75% selectivity. Oxygenates formed include ethylene oxide (CH_3CHO), formaldehyde (CH_2O) and methanol (CH_3OH) [21]. Formation of oxygenates is chemistry specific, and in their work, Iorganoglou and Schmidt noticed that nitrogen dilution lowered the oxygenate formation and that a coarser mesh gauze gave higher oxygenate yield than a finer mesh. In addition, they observed multiple steady states, perhaps due to the strong homogeneous and heterogeneous coupling that leads to non-equilibrium operation and oscillations as predicted by Song et al [22].

Wanat et al investigated the partial oxidation of alcohols (1-propanol and 2-propanol with methanol and ethanol with several additives) at short contact time. In one set of experiments, all alcohols produced H_2 selectivities around 70-90% over Rh-Ce and Rh [23]. In contrast, 1-propanol and 2-propanol gave less syngas and up to 60% selectivity to oxygenates. From this seemingly strange behavior, they concluded that the selectivities obtained in CPO of alcohols varied strongly with size and structure of the alcohol. Methanol and ethanol produced snygas, probably because they react rapidly on the surface, but propanol (and probably higher alcohols) could give large amounts of oxygenates through suitable adjustment of carbon to oxygen ratios [23]. In their study, mostly produced was propanal (CH_3CH_2CHO) and acetone ($OC(CH_3)_2$). Again, it

showed the versatility of CPO reactors where the reaction pattern and excellent product distribution can be tailored by changing parameters such as catalyst support, feed and flow conditions and contact time.

1.5.3 CPO to Valuable Chemicals and Fuels

A valuable fuel, isobutylene, is a key component of methyl tertiary butyl ether (MTBE), a chemical used as an oxygenate for reformulated gasoline. Industrially, it is produced by the endothermic dehydrogenation of isobutene over Cr_2O_3-Al_2O_3 catalyst at 1s residence time. While isobutylene selectivity is almost 100%, the fuel conversion is less than 5 % [24]. As such, Liebmann and Schmidt performed experiments on the oxidative dehydrogenation of isobutene on noble metal coated ceramic foam monoliths in a CPO reactor. Isobutylene and propylene were produced with selectivities exceeding 70% at 70% fuel conversion on Pt/Al_2O_3 catalyst [25]. Experiments they performed at higher space velocities showed that the selectivity to isobutylene increases at the expense of propylene. While certainly not optimal in comparison to industrial performance, it provided an alternative as no coking occurred and the need external heat was eliminated.

Bharadwaj and Schmidt investigated the production of ethylene or syngas from ethane as well as olefins from propane and *n*-butane, both over Pt. Respectively, ethylene and propylene were produced at 55-60% and 65-70% selectivity from *n*-butane [26]. Results with propane were very similar. After varying pre-heat conditions and other parameters, they concluded that ethylene production dominates at high temperature and longer contact time, while propylene production is maximized at lower temperatures and shorter contact time. The other concept illustrated was the extension of CPO reactors to an operational form mimicking that of a static fluidized bed reactor over alumina beads.

The valuable olefin production concept was extended to higher hydrocarbons as seen in the work of Krummenacher et al where *n*-decane was introduced at short contact times, comparing Pt and Rh performance. Over Rh, high H_2 selectivity was obtained when an alumina wash coat was added while the absence of wash coat and a larger pore size gave more olefins (up to 60%). Pt-Rh gave much higher selectivities to olefins than

either metal, maximizing at 89% [27]. The extension of this concept adds merit once more to how the CPO reactor concept is highly tunable. The high activity of Rh, which removes O_2 early in the catalyst, was combined with a low oxidative ability of Pt to produce a robust bimetallic catalyst.

1.6 Background on the Oxidative Dehydrogenation of Ethane

The oxidative dehydrogenation of ethane (ODH) to ethylene at short contact times has been shown to give selectivities as good as steam cracking as will be discussed in this section. A CPO ratio below, when applied to partial oxidation of ethane, is called ODH. The overall ODH reaction proceeds as follows:

$$C_2H_6 + \frac{1}{2}O_2 \rightarrow C_2H_4 + H_2O \qquad \Delta H^o = -105 \text{ kJ/mol} \qquad (1.4)$$

The overall reaction is exothermic; hence the reaction essentially drives itself, making ODH autothermal.

1.6.1 Brief Literature Review

ODH of ethane and ways to optimize it in a CPO reactor have been studied in the Schmidt group and other groups for the last 15 years. ODH had been studied previously over oxide catalysts but the processes were known to be selective to C_2H_4 at very low ethane conversion [28, 29]. In addition, oxidation of alkanes was unselective, resulting in an array of possibilities such as complete combustion, syngas formation, cracking or dehydrogenation reactions. Huff et al were therefore motivated find conditions under which syngas formation was dominant and when other gaseous products were selectively formed by ODH of ethane (methane and propane feeds were also studied) at short contact time on Pt, Rh and Pd. They obtained selectivities to C_2H_4 up to 30% with 50% ethane conversion on Pt under fuel rich conditions, while Rh produced high selectivities to syngas and Pd coked heavily then extinguished [30]. In a different set of experiments,

Huff and Schimdt revisited ODH, focusing primarily on ethane and using air stoichiometry as practiced in industry. Selectivities to ethylene up to 70% were obtained at 80% fuel conversion and 40% yield [31].

Adopting Huff's experiment, Yokoyama et al investigated the effect of adding various metals to Pt coated monoliths for ODH. The bimetallic catalysts prepared formed a Pt-M complex, were the M included Sn, Cu, Ag, Mg, Ce, La, Ni, Co and Au. They concluded that the addition of Sn or Cu gave the best performance by enhancing ethane conversion and olefin selectivities while suppressing CO_x formation [32]. While selectivity to ethylene was similar to Huff et al, a 50% yield was obtained making Pt-Sn superior than Pt alone. In the same paper, Yokoyama et al postulated that selectivity to ethylene required either acceleration of β-hydrogen elimination relative to α-hydrogen elimination (which produces methane and CO_x) and/or acceleration of the rate of C_2H_4 (ad) desorption relative to further reaction on the surface. The later possibility seemed more plausible for the Pt-Sn catalyst, hence its superior performance [32].

Bodke et al then investigated the effect of H_2 addition following insights from patents that suggested addition of H_2 with noble metal catalyst could increase performance in oxidative dehydrogenation. When hydrogen is added to ethane ODH, the reaction is hypothesized as a two-step process of hydrogen oxidation followed by ethane dehydrogenation as follows:

$$H_2 + \frac{1}{2}O_2 \rightarrow H_2O \qquad \Delta H^o = -241.8 \text{ kJ/mol} \qquad (1.5)$$

$$C_2H_6 \rightarrow C_2H_4 + H_2 \qquad \Delta H^o = +136.8 \text{ kJ/mol} \qquad (1.6)$$

The sum of the endothermic hydrogen oxidation and endothermic ethane dehydrogenation yields the ODH reaction (equation 1.4). With hydrogen addition, selectivities up to 85% for ethylene were obtained using a Pt-Sn catalyst operating at 950^{o}C and 1 ms contact time [33]. Production of undesired CO and CO_2 was reduced from 20% with no H_2 addition to 5% when hydrogen was added. Although the 2/2/1 $C_2H_6/H_2/O_2$ mixture is supposed to be explosive at the operating temperatures, no flames

or explosions occurred in the presence of ethane [33]. In this study, the catalyst was ignited with a Bunsen burner flame, after which the burner was removed and the reaction zone insulated to achieve nearly adiabatic conditions.

1.7 Questions Leading to Research Motivation

Consequently, these findings attested ODH in a CPO reactor gave comparable performance to steam cracking and showed great promise for commercial application, especially considering the value and importance of ethylene. However, for the ODH system, no one fully understood and could attest to the mechanism (which is critical for maximizing ethylene production) of how these non-equilibrium products were formed, a major motivation for this work. Several theories have been proposed as noted in the following section.

1.7.1 Proposed Mechanisms for ODH

1. Pure Homogeneous Mechanisms

Huff and Schmidt developed a 24-step model of adsorption, desorption and surface reactions where the reaction parameters for the elementary steps were obtained from surface science and catalysis literature, while some were fit to experimental data based on their work two years earlier. The model agreed within reasonable limits with the experimental data, matching selectivity and conversion trends [34]. It was enough to capture the main features of the reaction system, proposing that a purely heterogeneous model could be used to simulate experimental results obtained at atmospheric pressure. In essence, what happens is ethane dissociates into C_2H_5(ad) and OH(ad) on the surface. Then β-hydrogen elimination produces C_2H_4(ad), followed by a desorption step to form ethylene. α-hydrogen elimination of C_2H_5(ad) produced CH_4 and COx. Schematically , it is depicted in Figure 1-3.

The model did not however incorporate mass transfer limitations from the bulk to the surface, on the boundary layer and back to the bulk. Hickman and Schmidt had proposed a heterogeneous model on methane that accounted for the existence of mass transfer limitations [35]. Because mass transfer coefficients greater that 1000 cm/s do not affect reaction rates and product distribution as proposed by Hickman and Schmidt, the heterogeneous model set the dissociative adsorption steps at the flux limit to account for mass transfer limitations. This was because surface reactions are extremely fast compared to the gas-phase adsorption steps, therefore the reaction rates are limited by the flux of the reactants to the surface [34]. A major problem associated with this mechanism is that most of the oxygen was consumed in the first few mm of the catalyst. Oxygen is necessary at each step of the adsorption/desorption scheme to produce the large selectivity to ethylene. Hence due to the fact that ethylene was produced in the absence of oxygen, a homogeneous scheme is also likely.

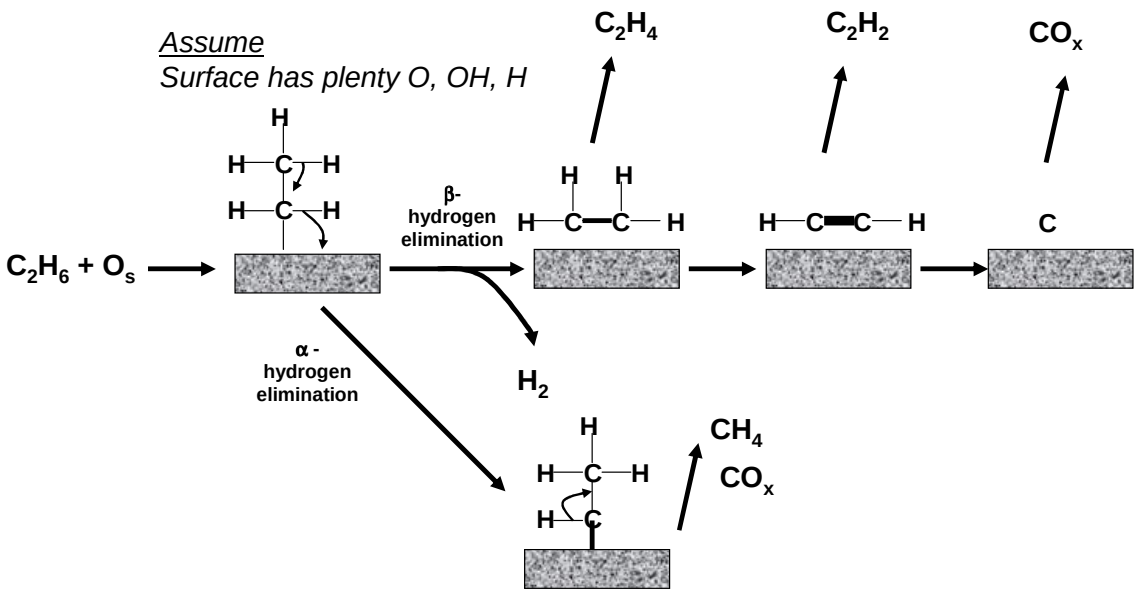

Figure 1- 3: Heterogeneous reaction mechanism as proposed by Huff and Schmidt.

2. Pure Homogenous Mechanism

Purely homogenous reactions have been analyzed in a detailed gas-phase hydrocarbon oxidation model that uses and encompasses extensive knowledge in the pyrolysis and oxidation of hydrocarbons. It contains more than 150 radicals and molecules, with a span of over 3000 elementary and lumped reactions [36]. The chemistry of a wide variety of C species, as high as C10's, was compounded into the reaction scheme. Model predictions were compared to data obtained in pyrolysis, partial oxidation and combustion experiments. Complex, multiple and consecutive free radical chain mechanisms are responsible for gas phase pyrolysis once the initial radical pool is formed. The remainder of the reaction scheme proceeds via H-abstraction reactions; hydrogen and methyl radicals prevail in pyrolysis and combustion, hydroxyl and hydroperoxy radicals play a major role in oxidation conditions [36]. The scheme can be thought to proceed as follows:

$$C_2H_6 + OH \rightleftharpoons H_2O + C_2H_5\bullet$$
$$C_2H_6 + H\bullet \rightleftharpoons H_2 + C_2H_5\bullet$$
$$C_2H_6 + \bullet CH_3 \rightleftharpoons CH_4 + C_2H_5\bullet$$
$$C_2H_5\bullet + OH \rightleftharpoons H_2O + C_2H_4$$
$$C_2H_4 + OH \rightleftharpoons H_2O + C_2H_3\bullet$$
$$C_2H_3\bullet + OH \rightleftharpoons H_2O + C_2H_2$$
$$...etc$$

Figure 1- 4: Reaction scheme in homogeneous pyrolysis.

This is in agreement with work done by Silberova et al where ODH was done under conventional microreactor and Temporal Analysis of Products (TAP) conditions over Pt on alumina at millisecond contact time. While the temperatures under study were only up to 600^{o}C, they found no evidence of ethylene formation during TAP conditions, whereas some ethylene was produced under flow conditions [37] consistent with gas phase production rather than surface mechanism. From the TAP experiments, it was clear that although oxygen increased the reaction rate of ethane on the catalyst, the presence of oxygen was not required to activate ethane at low temperatures. Beretta et al saw the same phenomenon when ethane ODH was performed with a comparative

analysis between catalytic tests vs. tests in an empty reactor, concluding that homogenous reactions played a fundamental role in high temperature production of olefins. In essence, they found no evidence of catalytic production of ethane. Combining the results of a theoretical analysis on homogeneous ethane oxidative pyrolysis, their results indicated that the high-temperature production of ethylene observed in the presence of the catalyst could be well explained by the single contribution of gas-phase radical reactions [38]. The catalyst was confirmed to be highly active, instead, in then non-selective oxidation of paraffins to CO_x.

3. Combined Homogeneous and Heterogeneous Mechanism

Zerkel et al did experiments specifically aimed at understanding reaction pathways of ODH over Pt in a short contact time reactor. An 82-step reaction mechanism was proposed using a 2D fluid mechanics model with full heat and mass transport treatment. They employed detailed homogenous and heterogeneous reaction schemes to describe the chemistry of ODH. Rate constants for elementary reaction steps were determined from literature as well as fitting model predictions to experimental data. In these simulations, Zerkel et al concluded that platinum catalyzed reaction schemes had heterogeneous processes responsible for oxidizing surface carbon and hydrogen, resulting in localized heat release into the gas phase. This heat was then responsible for driving endothermic homogenous and heterogeneous cracking of ethane to ethylene. A good fit was obtained between experimental data and model predictions at all ethane/oxygen mixtures. They argued that while unequal homogenous and heterogeneous contributions exist, their proportional contributions are largely dependent on reactor operating conditions [39].

Beretta et al also did a different set of experiments to better elucidate the role of gas phase reactions and surface catalysis. Their results suggested that maximum reactor performance relied on synergism between catalytic reactions (responsible for deep oxidation and partial oxidation to CO_x, H_2O and H_2) and homogeneous reactions (responsible for olefin formation). Thus, under autothermal conditions, they believed that

the catalyst accelerated ignition of the radical process through the initial combustion of ethane which can happen as low as 200^{o}C [40]. Huff et al later revisited ODH and reached a similar conclusion. They believed that overall, the system can be viewed as one in which the catalyst initiates gas-phase chemistry through the acceleration of exothermic reactions at the front of the reactor which increase the downstream temperature to the point where gas-phase reactions occur readily [41].

Recently, work by Vincent et al captures surface chemistry derived from four reaction classes: direct adsorption, adsorption on an adsorbate, surface reactions with adsorbed reactants and unimolecular surface reactions including desorption. The Unity Bond Index–Quadratic Exponential Potential (UBI–QEP) method was combined with collision theory from Density Functional Theory (DFT) studies to provide a basis for the semi-automatic generation of two consistent heterogeneous reaction mechanisms. Their work allows a more comprehensive assessment of the relative contributions of homogeneous and heterogeneous chemical processes. It is shown that the simulations capture all experimental trends with reasonable quantitative accuracy. The results of the study suggest that the catalytic dehydrogenation of C_2H_6 initially contributes to the net production of C_2H_4 and that changing conditions in the gas phase adjacent to the catalyst can result in the consumption of ethylene principally leading to methane and carbon deposition [42]. Homogenous reactions are thought to play a role following depletion of oxygen.

Considering that CPO has proved quite promising as a replacement for steam cracking with several advantages, understanding the ins and outs of reaction chemistry that occurs is vital in optimizing its performance, tailoring end products and scale up. Given the complexities associated with foam monoliths, high reaction temperatures and short contact time, analyzing just the reactor effluents is not sufficient. To truly understand the roles of oxidative and non-oxidative chemistry, decipher contributions from homogeneous and heterogeneous processes like so, quantify and qualify product evolution and explore ideal operating conditions, the spatial profiling technique is used to gain insight.

1.8 Introduction to Spatially Resolved Measurements

Since the introduction of catalysis and reaction engineering, reactors have essentially operated using primarily effluent data to decipher and propose what occurs inside them at relevant conditions. While extensive research has been done to tailor end product distribution, even simple systems such as methane oxidation to syngas are not understood and much controversy still exists in literature as to whether direct (pyrolysis-oxidation) or indirect (combustion-reforming) mechanisms are responsible for product formation [43].

Part of the reason why product evolution along the catalyst has been difficult to measure is because of the high temperature gradients in CPO reactors (as much as 200^{o}C/mm) and the extremely short contact time. Some attempts have been done using thermowells as well as infra red (IR) cameras to collect axial temperature profiles [44-46], but these experiments introduced heat loss by conduction and radiation as compared to fully insulated monoliths. Henning and Schmidt did experiments where they could not access the catalyst profile extensively (only 3 points were taken), hence instead, they used multiple reactor side ports where GC injections were taken to find species and temperature profiles within and after the catalyst [47]. Again, the technique lacked the spatial resolution needed and the existence of multiple reactor side ports potentially disturbed the system.

Horn et al devised a way to access and acquire product evolution inside the catalyst with a resolution of <0.3 mm. This technique, termed spatially resolved measurements, allowed for the first time, a precise and detailed look inside the monoliths, capturing axial species and temperature profiles with negligible disturbance [48]. Spatially resolved data can then be used to verify simulations, capture true mechanisms along the catalyst and optimize catalytic systems. Most importantly, being able to capture species evolution and transport phenomena in situ, at the industrially relevant conditions, is unequivocal in validating modeling efforts.

As will be discussed in detail in Chapter 2, the technique involves drilling a hole at the center of the monolith. The 3 monoliths (front heat shield, catalyst, back heat

shield) are lined up so that the holes are collinear. A chemically inert high temperature resistant fused silica capillary, similar to one used in a gas chromatograph column, is placed through the hole in the monoliths. This leaves an annular distance which is significantly lower than the average pore size of monoliths used. The capillary is connected to a microvolume tee that is attached to a stepper motor which enables linear translation up and down the monolith channel. Gases were sampled axially along the catalysts at flow rates much less than the total flow rate through the reactor to a mass spectrometer and gas chromatograph for species analysis and quantification. Temperature profiles were also measured by inserting a fiber optic probe and thermocouple into the capillary.

ODH, because of its extraordinary importance and relevance, will be examined using spatially resolved measurements so as to gain insight on product evolution and provide data to help validate, if not improve, existing models. It may be able to add valuable data that will contribute to a pool of knowledge in attempting to settle the ongoing debate about the true and complete mechanism of ethane ODH.

Chapter 2

Experimental

2.1 Summary

In this chapter, monolithic foams are introduced and concepts surrounding their properties, manufacture and applications to short contact time reactors are given. The incipient wetness technique is described as it applies to catalyst preparation and conditioning. Afterwards, the spatial profiles technique is discussed in great detail. Reactor schematic and monolith setup follow. Next, an explanation of how analysis is done by both a quadrupole mass spectrometer as well as gas chromatograph is given. Details surrounding temperature measurement by both a thermocouple and an optical pyrometer are presented, after which the experimental procedure used is outlined.

2.2 Introduction to Monoliths

Numerous industrial catalytic processes are highly exothermic, with examples such as hydrogenation, alkylation, partial oxidation and Fisher Tropsch synthesis. Most of these processes have heat transfer limitations. To account for these limitations, multiple reactor tubes of smaller diameter to increase heat transfer area are incorporated [49]. As a result, the catalyst pellets that are used are larger in diameter to compensate for the large pressure drops encountered. While radial heat transfer is increased, the effectiveness factor decreases and more catalyst is required [49]. This is not as much of a problem as the serious consequences that occur when heat released by the reaction is not removed quickly enough. Hot spots develop at the center of the tubes resulting in explosions, deactivation of catalyst through sintering or other thermal effects. This lowers selectivity, increases uncontrolled side reactions and in extreme cases, causes reactor runaway.

Reticulated ceramic foams (monoliths), in the form of cylindrical cartridges, are designed to help alleviate the problems aforementioned. Reticulated ceramics are materials consisting of two continuous phases; the ceramic and porosity. The most popular way to prepare foams involves loading a separately preformed foamed plastic shape with an aqueous oxide slurry that is then dried and calcined [50, 51]. Generally, polyurethane foam shapes are used, where the pores of the foamed polymer are filled with aqueous slurry of ceramic (α-Al_2O_3 (alumina), ZrO_2, etc) consisting of 0.1 – 10 μm diameter particles with small amounts of wetting agents, dispersion stabilizers and viscosity modifiers. To remove excess slurry, one can squeeze or air is blown through the foam, after which it is dried and calcined at temperatures in excess of 1000^{o}C [49]. During calcining, the plastic burns out and ceramic particles sinter, thereby forming a replica of the original plastic foam. The result is a macroporous structure consisting of cells, windows, struts, internal voids and microporosity as shown in Figure 2.1. The unique 3D structure and internal pore remnants from processing make the mechanical characterization and modeling of reticulated forms extremely difficult [52].

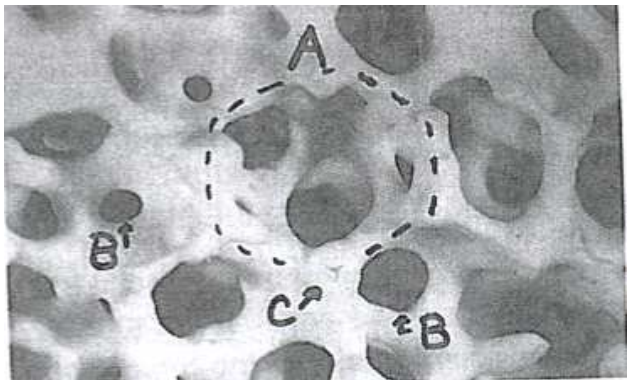

A=Cell B=Pore (Window)

C=Strut with internal void from precursor burnout

Individual Unit Cell

Figure 2- 1: Depiction of microporous structure in foams (adopted from Strom et al)

Most research and industrial applications encountered to date for reticulated ceramics utilize materials in the 10-100 PPI range. PPI refers to pores per linear inch, but because of the difficulties in accurately and efficiently measuring PPI, it is used as a relative designation rather than an exact value [52]. Due to their high porosity, they are very lightweight, rigid and self-supporting and can be used as catalytic bed supports for other materials. They have a flow through capability, implying liquids and gases can flow with minimal resistance, hence the low pressure drop (typically less that 1" of water column) [52]. Richardson et al developed pressure correlations for foams and found that a reduction of a factor of 10 is noticed in pressure drop compared to equivalent pellets [53]. The diffusion length for the monolithic reactor can therefore be chosen to be in the micrometer range, whereas for a sphere, the minimal dimension in a packed bed will be on the order of several millimeters in order to have acceptable pressure drops [54]. The advantage of the monolith becomes clear.

These ceramic foam monoliths, because of their properties, have been noted as very promising to industrial catalytic processes [49]. These processes generally fall into the following categories: heat transfer limited processes, pore diffusion limited processes and those with selectivity problems. As the gaseous or liquid medium flows through the reticulate, it is forced to divide and recombine in the struts, resulting in very efficient

mixing and high surface interaction, resulting in better radial heat transfer and high effectiveness. Due to high transparency to radiation of the solid phase, in particular at high temperatures, an important heat transfer mechanism in foam monoliths is radiation scattering. The effective thermal conductivity of Al_2O_3 monoliths used here is less than 1 W/m K for temperatures up to 1500^oC [55].

Peng et al also demonstrated that 1-D and 2-D heat transfer coefficients were higher on monoliths by a factor of five or more than of equivalent pellets. Catalysts operating in pore diffusion limited regimes require small pellets to increase the surface area to volume ratio. This leads to a larger pressure drop, yet reticulated foams give improved effectiveness and lower pressure drop [56]. The high surface area of reticulate foam is important in terms of chemical or catalytic reactions. Surface area can be improved by addition of wash coat. Wash coat refers to the application of a fine-grained coating (e.g. γ-alumina, ceria) to the ceramic and has been found to increase surface areas of reticulates from 1-2 m^2g^{-1} to above 30 m^2g^{-1}, closely matching areas of conventional catalysts that have a range of 50-200 m^2g^{-1} [49, 57].

In summary, reticulated ceramic foams are desirable because of the following; low pressure drop since porosities are high, high surface area resulting in effective external mass transfer and large effectiveness for pore diffusion limited regimes, excellent mixing resulting in improved convective heat transfer and enhanced radiation within the bed because of higher void spaces. Properties of the monoliths used in this work are noted below [49].

Source	High-Tech Ceramics, Alfred, NY
Material	99.5% α-Al_2O_3,0.5% mullite
Pore Density	45 PPI
Pore Diameter	0.42 mm
Bulk Density	0.65 g cm^{-3}
Porosity	0.84
External Surface Area	$6.21*10^{-4}$ m^2m^{-3}(solid)

Table 2- 1: Typical monolith properties used during the ODH of C_2H_6.

2.3 Capillary Sampling Technique

Using an ultra sonic drill, a 740 µm hole is drilled along the centerline of the monolith using a diamond tipped drill bit. The 3 monoliths, front heat shield (FHS), catalyst and back heat shield (BHS), are lined up so that the holes are collinear (see Figure 2.2). A fused silica capillary, similar to one used in a gas chromatograph, of size 640 µm outer diameter and 540 µm inner diameter, is placed through the hole in the monoliths. This leaves an annular distance of about 100 µm, which is significantly lower than the average pore size of monoliths (430 µm). Fused silica is known to be chemically inert, has nearly zero thermal expansion, exhibits exceptionally good thermal shock resistance, can be lapped and polished into fine finishes and has superb transparency to radiation. In addition, its softening point is around 1600^{o}C, making it suitable for CPO reaction conditions with minimal disturbance to the reactor system.

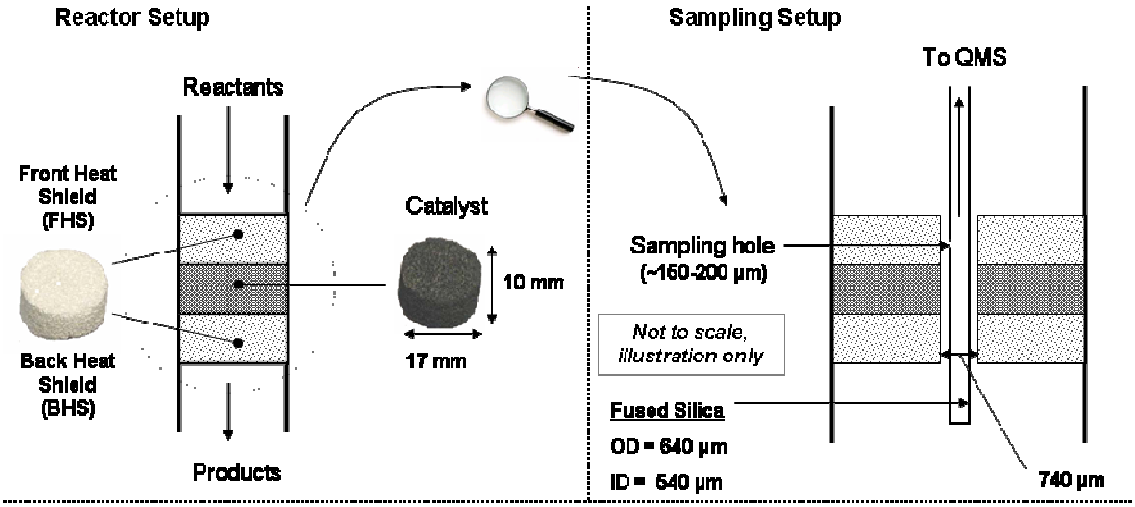

Figure 2- 2: Illustration of reactor and monolith setup for gas sampling.

The capillary is connected to a microvolume tee (Valco), which is attached to a stepper motor (Zaber Technologies) controlled by LabView. Linear translation up and down the monolith channel is done using the stepper motor which has accuracy to of ±16 µm and can move with speeds as slow as 0.0009 mm/s. It has a repeatability of < 0.4 µm and a range of 60 mm. To prepare the capillary for sampling, a small hole was cut by hand under a magnifying glass using a ceramic scribe. Care has to be taken to the silica

capillary as it become very brittle from stress applied and cracks formed during the scribing process. The polyimide polymer surrounding the capillary is burnt off using a torch and the hole is annealed to relax the stress and weakening cracks. Great care must then be taken when inserting the capillary through the monoliths as any slight misalignment of the foams will create a tortuous path that puts additional stress, forcing it to break.

The front end of the capillary (about 40 mm away from the hole) is torched using a micronox torch with butane and nitrous oxide as the oxidizer until it softens and closes itself. This is to ensure gases are only sampled from the hole that is manually cut while taking spatial profiles. The polyimide polymer covering a 30-35 mm section above the hole is burnt away to avoid polymer depositing onto the catalyst or heat shields. Species are then sampled through the hole, into the capillary, then the microvolume tee connected to a metering valve to adjust flowrate, and finally through a 1/16" OD and 0.01" ID stainless steel tubing that directs flow to a quadrupole mass spectrometer (QMS) for analysis and quantitative species determination.

2.4 Catalyst Preparation, Reduction and Conditioning

The monoliths used in this study are α-Al_2O_3 (99.5%) foam monoliths (~10 mm long and 17 mm in diameter, 45 ppi, Vesuvius Hi-Tech Ceramics). An ultrasonic drill was used drill to the hole for the sampling capillary along the monolith centerline, where a wax was applied to glue them steady while drilling. Removal of this wax was done by rinsing the foam monoliths in acetone followed by calcining at 600^{o}C for 2.5 hours.

To load the blank monolith with catalyst, the incipient wetness impregnation was used. The incipient wetness impregnation constitutes filling the entire pore volume of catalytic support with a precursor solution without wetting the inter-particle void spaces with excess precursor solution. After impregnation, the metal precursor solution remains largely inside the pore. Upon subsequent drying and calcining, the precursors typically decompose to metal-oxides. Generally, the incipient wetness point (i.e. the amount of liquid added just equals the water accessible pore volume of the solid) can be determined

by N_2 adsorption-desoption in a BET measurement or simply by visual inspection using a solvent (e.g., de-ionized water) as the liquid medium. On conventional catalytic supports such as SiO_2 or Al_2O_3, the incipient wetness points are usually found to be independent of the precursor loading in the precursor solution [58].

For monometallic catalysts, Rh ones were prepared by wetting the monoliths to the incipient point with an aqueous solution of $Rh(NO_3)_3$ (Alfa Aesar) containing enough Rh atoms to produce a final metal loading of 4.7 wt%. The monoliths were then dried in air over night, after which they were calcined at 600 ºC for 2 h. To make the second monometallic catalyst, Pt was deposited from H_2PtCl_6 solutions (Alfa Aesar), and heat treated as described above. Both catalysts were treated in flowing H_2 (5% in Ar balance at 500 sccm) at 250 ºC for 2 h prior to use.

For bimetallic catalysts, Pt was loaded from H_2PtCl_6 solutions (Alfa Aesar) followed by vacuum drying at room temperature overnight, after which they were calcined for 6 hours at 600^{o}C. Tin was added in a similar manner to Pt except from $SnBr_2$ (Alfa Aesar) solutions and oven treatment at 700^{o}C. Copper was added from $Cu(NO_3)_2.6H_2O$ (Alfa Aesar) solutions and treated similary as the Sn additions. The final metal loading was noted by differential weighing after the catalysts cooled, and was determined to be 2% Pt / 2 % other metal in both Sn and Cu cases. Once the second metal was loaded, the catalysts were treated using temperature programmed reduction at 10^{o}C/min up to 900^{o}C in a 1 SLPM flow of 10% H_2 and balance Ar and maintained for 0.5 hours at maximum temperature.

For first time light-off with monometallics, a mixture of Ar (3 SLPM), H_2 (0.4 SLPM) and O_2 (0.2 SLPM) was sufficient to increase the temperature in excess of 350^{o}C following which a switch was made between gases to the experimental stoichiometry being studied. However a different method was used for bimetallics as the one mentioned before did not work. For first time light off with bimetallics, a mixture of CH_4 and O_2 was first used to raise the temperature to >600^{o}C and the alkane was slowly switched to C_2H_6. The differences in light-off are attributed to different metallic states and reduction points between Pt alone and bimetallic combinations.

To condition the catalysts and avoid variability in performance, they were operated at extreme experimental conditions experienced i.e. high and low carbon to oxygen ratio (C/O) for 3 hours at each stoichiometry, then shutdown. Thereafter, light-off was performed normally starting with H_2 oxidation and then switching to C_2H_6 in air stoichiometry for C/O ratios from 1 to 2 in 0.2 increments, with and without H_2 addition. Total flow was maintained at 5 SLPM in all tests conducted.

2.5 Reactor Configuration and Monolith Setup

The reactor configuration used in this work is shown in Figure 2.3 on the next page, while the monolith setup was already shown in Figure 2-2. Before being inserted into the reactor, the monoliths are wrapped with a thin film of alumino silicate paper (Fiberax) to serve two purposes; to ensure a tight seal since the ID of the reactor is slightly larger than that of the monolith (hence minimizing gas bypass around the monoliths channels) and to keep the monoliths in a rigid position so the fragile sampling capillary can slide up and down a consistent path.

The grade and supplier of gases used were as follows: C_2H_6 (CP grade, Airgas North Central), O_2 (UHP Zero grade, Minneapolis Oxygen), H_2 (UPC grade, Minneapolis Oxygen), Ar (UPC grade, Minneapolis Oxygen), CO_2 (UPC grade, Minneapolis Oxygen), CH_4 (CP grade, Minneapolis Oxygen), C_2H_4 (CP grade, Airgas North Central), CO (CP grade, Matheson Tri-Gases) and C_2H_4 (AA grade, Minneapolis Oxygen).

The reactant gases are introduced from cylinder tanks via mass flow controllers (Brookfield) using 316 stainless steel tubing. O_2 is mixed with an Ar (inert) before being mixed with fuel in the pre-heater. The temperature in the pre-heater is kept at approximately 100^oC using a PID controller (Omega) where the input to the controller is a thermocouple (K-Type, Omega) placed on the reactor side port (approximately 30 mm above catalyst bed). Pre-heating above the catalyst surface not only helps with increasing reactants' energetics for autothermal operation, but serves primarily to prevent H_2O condensation since it is the cold side of the reactor through which hot gases sample through before getting to the QMS.

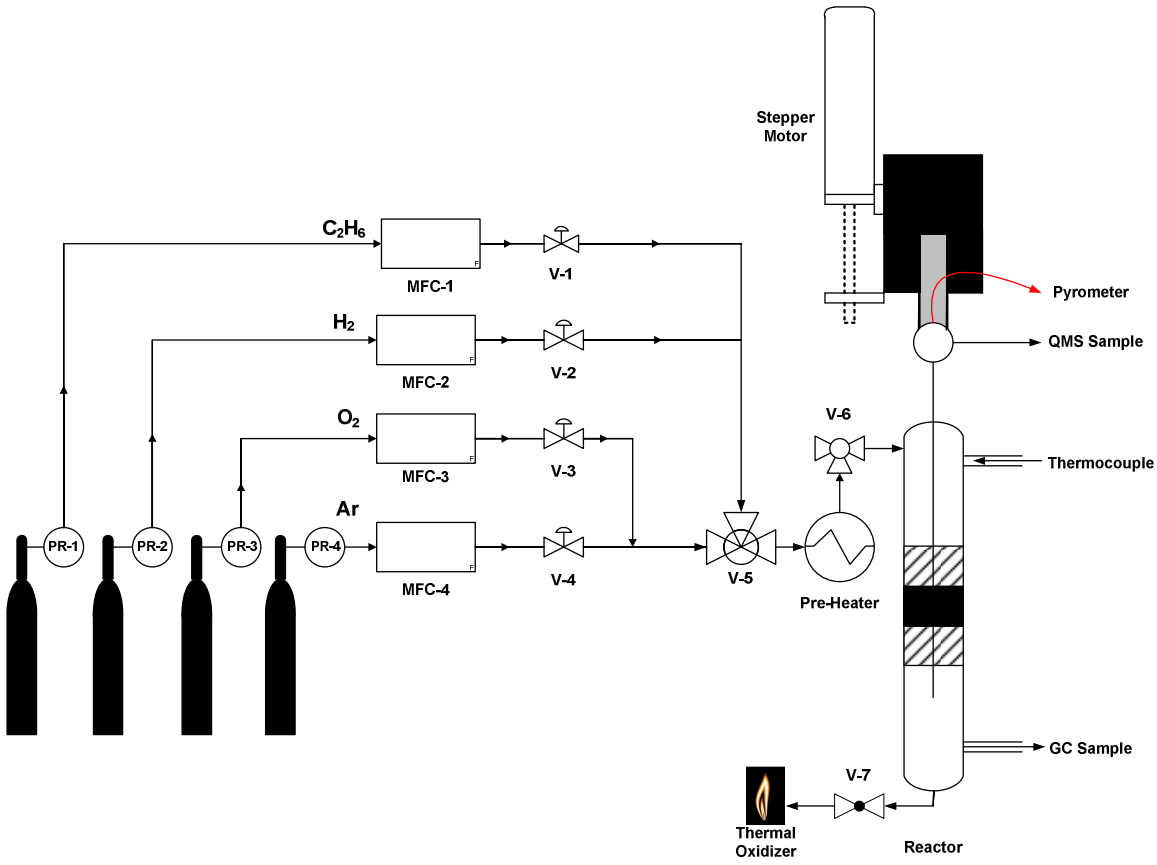

Figure 2- 3: Experimental setup used in the ODH of C_2H_6.

Downstream of the reactor, a GC sample is located approximately 40 mm below the FHS i.e. the non-catalytic portion of the reactor. The volumetric flow rate through this sample line is varied using a metering valve (Swagelok) since ODH of ethane has significant homogenous contributions and reactions tend to occur in the capillary at certain residence times. While sampling inside the capillary is a non-catalytic region, the temperatures at which the gases are sampled are known to be high enough to support homogenous chemistry [40]. As such, for consistency, the flow rate through this sample line is varied until fuel conversion in the QMS matches that obtained from the GC at the same axial location (40mm below the FHS). The capillary flow was then estimated ex situ with a small bubble column, and was found to be approximately 2% of the total reactor flow. Effluent from the reactor is send to a thermal oxidizer for incineration. User interface is aided by LabView.

2.6 Data Acquisition

In order to obtain species and temperature profiles, experimental data was acquired by the QMS, gas chromatograph, pyrometer and thermocouple as will be discussed next.

2.6.1 Data Acquisition by Quadrupole Mass Spectrometer (QMS)

The QMS used is a two stage differentially pumped system. It is an SRS Residual Gas Analyzer gas analyzer with a 70 eV electron ionizer, Faraday cup ion detector and a 16 stage electron multiplier. The first chamber is connected to a sapphire leak valve that is also connected to a six-way chamber. The six way chamber includes a transparent window for viewing inside the QMS, a thermocouple gauge, an ion gauge, a mechanical pump and the QMS. Opening the sapphire leak valve was done slowly until the pressure in the chamber reached a pressure on the order 10^{-7} torr. Ionization of gases is performed by the electron ionizer. It has thoriated-ruthenium filaments, and sends ionized gases to an electrometer. Ions that have the right mass to charge (m/z) ratio are considered stable, hence they reach the electrometer while those that have an incorrect m/z ratio are bombarded into the wall of the mass spectrometer. The current measured by the electrometer is amplified and sent to Labview.

A voltage ramp was programmed in LabView, with a scan over the following mass to charge ratio (m/z) common of ODH of ethane products: 2, 15, 16, 18, 20, 25, 26, 27, 28, 30, 32, 40 and 44. Several thousand samples were scanned and averaged during each sweep, producing a histogram or analog spectrum. Ar was used as the internal standard during calibration and all flows were normalized to Ar (i.e. $F_i = F/F_{Ar}$).

To check for linearity in the calibration as predicted by mass spectrometer theory, the following responses were checked:

$$k_i = \frac{S_i^{in} - S_i^{out}}{F_i^{in} - F_i^{out}} \qquad (2.1)$$

where k_i = response factor of species *i* at each m/z and its corresponding flows (F_i) and signal (S_i). The signal *i* was corrected for a blank signal when no analyte was present (i.e. $S_i = S_i$ - $blank_i$). The calculated response factors tend to drift slightly with time, but they are known to hold relatively constant. As such, to account for all the CPO of ethane species involved (H_2, O_2, Ar, CO, CH_4, CO_2, C_2H_2, C_2H_4, C_2H_6, H_2O), deconvolution of spectra signals was done. Some signals are unique and only have one m/z contribution.

Yet for other m/z, contributions are all coupled, hence deconvolution of the signal is needed. After using Equation 2.1 for isolated signals, the response factors for *i* at other m/z can be calculated as follows:

$$k_i^{'} = \left(\frac{k_i^{'}}{k_i} \right)_{matrix} * \; k_i \tag{2.2}$$

where matrix refers to values obtained from individual species calibration. For those signals that are not unique, their response factors are calculated by subtracting each signal at a specific m/z from the total signal for that m/z as follows:

$$k_i = \frac{(S_i^{in} - S_i^{out} - \sum_{i \neq j} k_{ij}(S_i^{in} - S_i^{out})}{F_i^{in} - F_i^{out}} \tag{2.3}$$

The same procedure was used when flows had to be calculated for given species in the spectral profile. The QMS is useful for analyzing fast transient effects because it has very fast response time, making it suitable for spatial profiles. For more accurate quantitative data analysis, a gas chromatograph is used. A typical normalized QMS fractionation pattern is shown in Table 2.2.

m/z	2	15	16	18	20	25	26	27	28	30	32	40	44
Ar	0	0	0	0	0.1000	0	0	0	0	0	0	1.0000	0
O_2	0	0	0.1728	0	0	0	0	0	0.0091	0	1.0000	0	0.0162
CO	0	0	0.0242	0	0	0	0	0	1.0000	0	0	0	0
CO_2	0	0	0.0929	0	0	0	0	0	0.1442	0	0	0	1.0000
H_2	1.0000	0	0	0	0	0	0	0	0	0	0	0	0
CH_4	0.0272	0.8314	1.0000	0	0	0	0	0	0	0	0	0	0
C_2H_2	0	0	0	0	0	0	1.0000	0	0	0	0	0	0
C_2H_4	0.0726	0	0	0	0	0.1245	0.6092	0.6084	1.0000	0	0	0	0
C_2H_6	0.0387	0.0575	0	0	0	0.0381	0.2357	0.3410	1.0000	0.2230	0	0	0
H_2O	0	0	0	1.0000	0	0	0	0	0	0	0	0	0

Table 2- 2: Typical QMS fractionation pattern during the ODH of C_2H_6.

2.6.2 Data Acquisition by Gas Chromatograph (GC)

The GC used is an HP 5890 equipped with a thermal conductivity detector (TCD) and a Hayesep D packed column (1/8" stainless steel). It also has automatic sample injection, cryogenic cooling and has automatic gas sampling controlled by a commercial software that provided user interface (HP Chemstation). Ar was used as the internal standard to account for volume expansion of reactions. Because it is inert, its flow rate is always known. High pressure He was used as the carrier gas. The use of Ar not only helped with data analysis as the QMS used the same standard, but leaks within the reactor setup and sampling lines could easily be detected should N_2 from air show up in the GC analysis.

To calibrate the GC, attempts were made to have partial pressures that produced species areas of the same size as those seen in the experiment. While response factors are supposed to be linear as dictated by chromatography theory, it is common practice to calibrate within experimental ranges for greater confidence and accuracy. Typically 3 replicates for 4-5 different ratios of flows of species i/Ar were injected into the GC. The flows are measured in replicates of 5 using a bubble column.

The response factors for permanent gases can be calculated as follows for Gaussian peaks:

$$RF_i = \left(\frac{A_{Ar}}{A_i}\right) * \left(\frac{F_i}{F_{Ar}}\right) \tag{2.4}$$

where RF is the response factor of species *i* and A_i and A_{Ar} are the areas of species *i* and Ar respectively. F_i and F_{Ar} are the flows of species *i* and Ar respectively. Column retention times were individually identified during calibration to accurately identify species during the experiment. Where possible, standard calibration cylinders were used to check the accuracy and validity of the performed calibrations, (ignoring concentration dependence) and were found to be within 5%. From the response factors calculated as stated above, and the flow rate of Ar that is always known, the flows for each species *i* when taking spatial profiles can then be calculated as follows:

$$F_i = RF_i * F_{Ar} * \left(\frac{A_i}{A_{Ar}}\right) \tag{2.5}$$

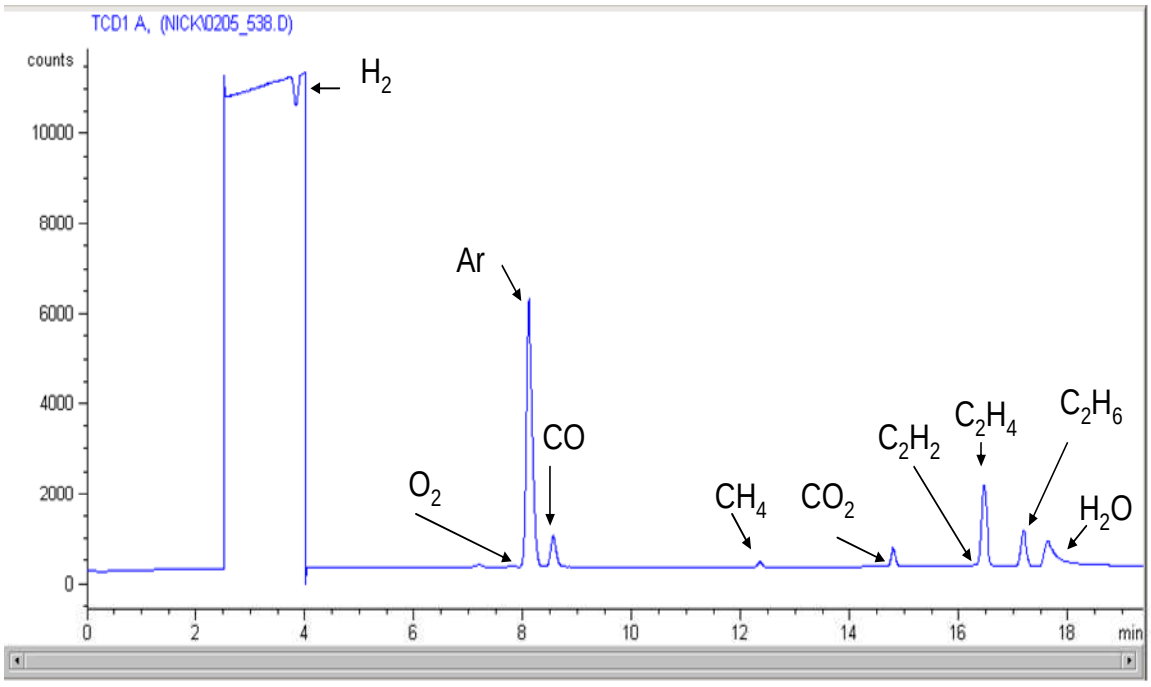

Figure 2- 4: Typical GC fractionation pattern seen during the ODH of C_2H_6.

The calculation of H_2O using the GC is unreliable due to contributions from condensation in the sample line, giving it a non-Gaussian peak. As such, the balance is closed on atomic O instead. To separate the permanent gases and H_2O, the cryogenic separation technique was used. The column was cooled using N_2 to -35^oC and held for 2 minutes after sample injection. The temperature in the column was increased at the rate of 7^oC/min until is reached 7^oC to allow for sensitive hydrogen separation. Following which the ramp was increased to 30^oC/min until a final temperature of 140^oC. This routine took approximately 22 minutes for all species to elute and was optimized to have the best separation as seen in a typical GC fraction pattern obtained shown before in Figure 2-4.

2.6.3 Data Acquisition Using a Pyrometer

An optical pyrometer (Mikron MI-GA5-LO), was used to approximate the catalyst surface temperature. It has a fiber optic for non-contact temperature measurement and is known to accurately work in the temperature range of 300–2500^oC using incandescent color. The theory behind optical pyrometers is that all black bodies have the same incandescent color at a given temperature. Pyrometers use a visual comparison between a calibrated light source and a targeted surface. When the filament or detector has the same temperature as the target, their thermal radiation intensity match and this causes the filament to disappear, blending in the background. The current passing through the filament at this time is converted into a temperature reading. Typical applications for pyrometers include welding, rotary kilns and annealing, where it is capable of measuring very short response times (less than 2ms).

The emissivity of optical pyrometers is adjustable depending on the object. MI-GA5-LO is capable of operating in emissivity range of 0.2-1. The upper end of the spectrum was assumed for temperature measurements taken in this work because the monolith geometry results in many internal reflections, approximating to that of a black body. Basically two groups of non-contact temperature measuring devices are available. Optical pyrometers measure the temperature in the visible spectrum of 0.4 - 0.7μm. The

second group, infrared thermometers, measure temperature in the infrared spectrum of 0.7 - 80µm. The MI-GA5-LO uses InGaAs as the infrared detector that has a spectral response of range 1.4 - 1.8µm with a resolution of <1^{o}C, hence strictly speaking, it would be considered an infrared thermometer.

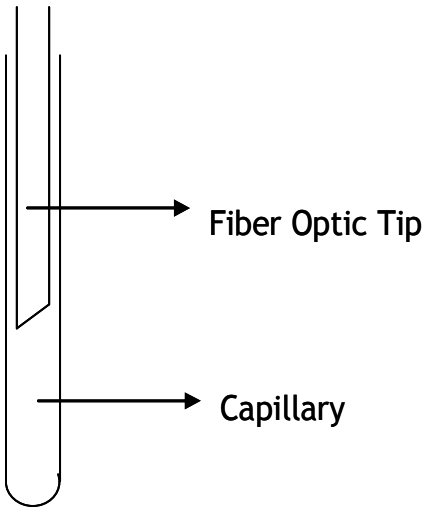

Figure 2- 5: Fiber optic placement for pyrometer temperature measurements.

A fused capillary is used to direct the fiber optic probe of the pyrometer down the monolith channel. The fiber optic tip has an OD of 330 µm, which fits nicely into the capillary (OD 640 µm). It is moved along the axis of the catalyst using a stepper motor while it measures surface temperature. The fused capillary is transparent to radiation at high temperatures, so the fiber optic directly views the catalyst surface. The end of the fiber is beveled at 45^{o} using a sandpaper so that the fiber collects radiation perpendicular to the axis of the fiber as illustrated in Figure 2-5 above.

2.6.4 Data Acquisition Using a Thermocouple

A thin diameter (OD 250 µm) inconel-sheathed K type thermocouple was placed in a thin fused capillary just like in the pyrometer measurements illustrated in Figure 2-5.

This was then placed from the bottom of the reactor such that it was barely touching the back heat shield. Because the thermocouple was enclosed in fused silica, and even if it may be touching the back heat shield, conduction along the thermocouple is minimal because it is so thin. As such, the temperature measured at that point is the best approximation of gas temperature flowing past it.

In contrast, if temperature measurements were to be done along the catalyst using a bare thermocouple, several scenarios can occur. The K type thermocouple has a thermal conductivity higher than that of the monolith, hence with extremely large temperature gradients inside the monolith, the thermocouple would axially and radially conduct heat away from the monolith. In addition, while coke formation has been shown to be negligible, when some carbon does deposit, it suppresses the temperature readings by reducing available thermocouple surface area. Exposure of this carbon to oxygen results in an exothermic reaction, producing CO and CO_2, which effectively increases the temperature until another monolayer of carbon (coke) deposits. As a result, the coking-decoking phenomena may give inaccurate readings that fluctuate due to endothermic coking and exothermic decoking.

2.7 Experimental Procedure

For the reactor to be completely setup, the following need to have been done:

✓ The three monoliths are aligned, alumino silicate paper is wrapped around them and a test capillary has already been slid up and down the drilled monolith channel to make sure no tension exists.

✓ Typically, a sampling capillary is used first. Therefore after cutting the hole, annealing and burning off the polymer, it is inserted into the monolith channel. A 50x microscope is used to locate the position of the hole, ensuring that it is slightly above the FHS. The stepper motor is used for linear translation and the starting position is noted.

✓ The reactor is then insulated using quartz wool (Fiberax), leak tested, sampling lines are turned on for resistive heating and the flow rates of the reactant gases are verified using a bubble column.

At this point, ethane CPO is ready to begin where a total flow rate of 5 standard liters per minute (SLPM) was consistently used. The following experimental procedure was followed:

Starting with monometallics procedure, a mixture of Ar (3 SLPM) and H_2 (O.4 SLPM) is introduced to allow for in-situ reduction of the catalysts, while the PID controller slowly increases the temperature to its preheat set point of 100^{o}C. The reduction procedure was allowed to continue until the pre-heat set point was reached, typically after 15 minutes. Oxygen (0.2 SLPM) was then introduced into the reactor and this oxidation reaction raised the catalyst temperature after light off to an excess of 350^{o}C. For bimetallics, after the preheat set point was met, a mixture of CH_4 (1 SLPM) and O_2 (0.2 SLPM) was introduced, raising the temperature to >600^{o}C after which the alkane was slowly switched to C_2H_6.

Next, the feed composition was changed to match the experimental conditions that needed to be studied. Approximately 2 hours was allowed after light-off to enable catalyst conditioning if it was being used for the first time. Once steady state was achieved, GC injections were taken and 4 replicates at each reaction condition were taken. Spatial profiles were taken a rate 0.01 mm/s. For temperature readings, the same procedure was followed except a different capillary was used as described in the preceding section 2.6.3 and 2.6.4. To shut off, O_2 was removed first, then C_2H_6. The pre-heater was switched off and the catalyst was cooled down in Ar. Once the temperature was less than 100^{o}C, Ar was switched off.

Chapter 3

ODH of Ethane on Pt and Rh

3.1 Summary

In this chapter, calculations to determine thermodynamic equilibrium product compositions are presented first, followed by adiabatic equilibrium calculations to check how well experimental reactor insulation was done. The integral results on Pt and Rh are discussed and compared. Noting that effluent data, while insightful, is not sufficient to explain the differences seen between the two catalysts, spatial profiles at low and high C/O are presented and discussed. Insights from these spatially resolved measurements suggest the type of reactions occurring, with results showing oxidation, combustion and reforming phenomena. Spatially resolved temperature profiles are given next. Realizing that raising the catalyst temperature in the front face may prove beneficial in promoting higher ethylene production as hypothesized before, spatial profiles showing the effect of H_2 addition are given. Mechanistic conclusions detailing Pt and Rh differences are then summarized.

3.2 ODH Equilibrium Considerations

Equilibrium calculations offer a practical way to observe the effects of process variables such as temperature, pressure and amounts of raw materials on product composition. HSC software [59] (commercially available), was used to perform equilibrium calculations. It does so using the Gibbs energy minimization technique. The problem of calculating equilibrium compositions is translated into determining the minimum of the total Gibbs free energy.

For a system with π phases and *n* components, it can be expressed as follows:

$$G = \sum_{s=1}^{\pi} \sum_{j=1}^{n} G_j^{(s)} N_j^{(s)} = \sum_{s=1}^{\pi} \sum_{j=1}^{n} \mu_j^{(s)} N_j^{(s)} \qquad (3.1)$$

Where $\mu_j^{(s)}$ is the chemical potential of all species. Element atomic balances are applied as conservation equations at any given fixed T and P. The stationary conditions for this minimization problem, which are well known in classical thermodynamics, equates the chemical potentials (and fugacities) of each species in all of the phases. For such non-linear systems, many solutions usually exist, only one of which is at the global minimum.

The minimization technique is similar to satisfying reaction constrains given for all reactions as follows [60]:

$$\sum_{j=1}^{n} v_{j,r} \mu_j^{(s)} = 0 \qquad (3.2)$$

Possible products considered as seen experimentally were O_2, Ar, CO, CH_4, CO_2, C_2H_2, C_2H_4, C_2H_6 and H_2O. HSC cannot solve adiabatic equilibrium; therefore equilibrium compositions were calculated at a wide range of temperatures. Using the enthalpy-temperature (H-T) diagram, the adiabatic compositions were determined to be the ones corresponding to a temperature where $\Delta H = 0$. Two cases were considered, one assuming all gas phase chemistry and the second one included possible formation of solid carbon. The equilibrium calculations plots are shown next, with the plot to the left (L) showing

results when only gas phase chemistry is considered. Whereas to the right (R), solid carbon formation is considered

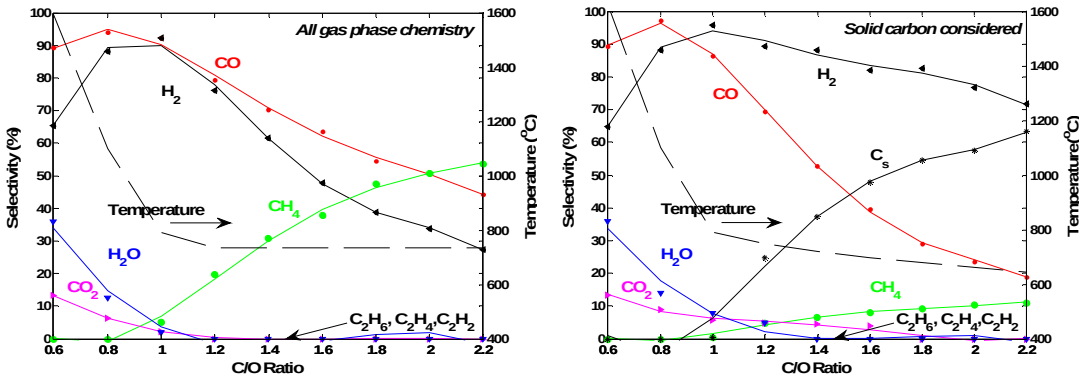

Figure 3- 1: Adiabatic equibrium calcuations for C_2H_6 ODH at 5 SLPM.

Product flow rates obtained from these calculations are when a total feed of 5 SLPM was considered. These selectivities can therefore be compared to other figures in the results section as the total feed was always the same. Syngas, and not ethylene, is predicted by equilibrium with complete conversion of C_2H_6 at all stoichiometries. Solid carbon is predicted to increase with increasing C/O ratio, with large amounts at C/O=2, where optimal ethylene production is obtained experimentally as will be shown later. Under experimental conditions studied, negligible carbon formation was observed (i.e. no reactor shutdown after several hours of operation) and atomic C balances always closed within ±5%. Atomic H balances also closed in the same range. Syngas and methane, rather than ethylene, is favored by thermodynamics.

3.2.1 Carbon Formation/Coking Phenomena in CPO Reactors

Given the fact that experimentally negligible coke formation was observed in this work performed in a CPO reactor, it is useful to understand why the ODH reaction selects for non-equilibrium products.

The definitions of carbon and coke are different, mostly in the convention relating to their origin. Carbon is a product of CO disproportionation (Boudouard reaction), while coke is produced by decomposition or condensation of hydrocarbons on metals [61]. The Boudouard reaction proceeds as follows:

$$2CO \rightarrow C_s + CO_2 \qquad \Delta H^o = -172 \text{ kJ/mol} \qquad (3.3)$$

However this forward reaction is only favored at temperatures below 700^{o}C [61], which are approximately 200^{o}C lower than those obtained experimentally in this work. In addition, Bartholomew argues that the presence of either H_2 or H_2O can reduce or eliminate the formation of coke or carbon by reacting with it to produce CH_4 or CO. If enough H_2 or H_2O is present, the surface residence time of active carbon species or coke precursors will be too short to allow measureable transformation of these species into more inactive forms [61]. As a result, the formation of condensed hydrocarbons and amorphous graphitic carbon in minimized. This reasoning is confirmed in spatially resolved measurements taken, as large amounts of H_2 and H_2O are present in the first 3 mm of all catalysts where a monolayer of carbon would likely form. Additionally, coke or carbon formation is suppressed by virtue of millisecond contact time since equilibrium conditions are not attained.

However, at elevated temperatures (>700^{o}C), ODH of C_2H_6 has other reactions that can produce coke namely C_2H_4 cracking and reverse steam reforming of carbon. Respectively, they occur as follows:

$$C_2H_4 \rightarrow 2C_s + 2H_2 \qquad \Delta H^o = -53 \text{ kJ/mol} \qquad (3.4)$$

$$CO + H_2 \rightarrow C_s + H_2O \qquad \Delta H^o = -171 \text{ kJ/mol} \qquad (3.5)$$

The equilibrium constants [31] for Equations 3.4 and 3.5 for the experimental conditions studied, say 900^{o}C, are $1.7*10^{-2}$ and $2.5*10^{-2}$ respectively. In contrast, the ODH of ethane reaction equilibrium constant is 6.2, orders of magnitude faster. Therefore the ODH reaction dominates. As such, carbon or coke formation is unfavorable because neither

equilibria for C_2H_4 cracking nor for reverse steam reforming of carbon is being driven thermodynamically to the right.

3.2.2 Reactor Adiabatic Temperatures

Since equilibrium compositions were not attained, it remained inconclusive as to whether the experimental heat balances were sufficient to drive the ODH reaction to equilibrium. As such, adiabatic reaction temperatures were also calculated. These are the theoretical temperatures that would be achieved under given conditions for specified feeds and products if there were no heat losses by conduction, convection or radiation. At high flow rates, the reactor approaches the limit of adiabatic operation and the autothermal temperature approaches the adiabatic operation temperature.

Within these limits, the first law becomes:

$$\sum_{i=1}^{n} Cp(T_{out} - T_{in}) = \sum_{i=1}^{n}(-\Delta H_i)X_i = 0 \qquad (3.6)$$

where $(-\Delta H_i)X_i$ is the sum of heats of reactions from both endothermic and exothermic chemistry at some average conversion X_i, $\sum_{i=1}^{n} Cp(T_{out} - T_{in})$ is the sensible temperature rise of the catalyst from T_{in} to the average catalyst temperature T_{out}.

	Pt		Rh	
C/O	T_{ad}	$T_{experimental}$	T_{ad}	$T_{experimental}$
1	1147	1040	930	910
1.2	1078	990	932	897
1.4	1025	962	919	885
1.6	990	943	897	873
1.8	945	930	876	861
2	937	916	872	854

Table 3- 1: Calculated C_2H_6 ODH adiabatic temperatures. Values in ^oC

Because equilibrium compositions were not achieved, experimental feed and product distributions were used as the input to HSC so as to find the adiabatic temperatures obtained when the heat balance was zero i.e. $\Delta H = 0$. The results are summarized in the Table 3.1. From these values, it can be inferred that the reactor insulation was excellent, as all values lie within 10% for Pt and 3% for Rh.

3.3 Results

3.3.1 Pt and Rh Integral Reactor Performance

To make an overall comparison in the reactor performance between Rh and Pt, integral reactor performance measured at axial position 12 mm below the FHS. Atomic selectivity to H and C, defined in the definitions section, as well as reactant conversion are all depicted in Figure 3-2. Here, it can be noted that C_2H_6 conversion decreases monotonically from 98% to 41% over the Pt catalyst and similarly decreases from 86% to 41% on Rh with increasing C/O from 1.0 to 2.0. Oxygen conversion is >99% over Rh for at every C/O whereas on Pt, it decreases from 97% to 85% with C/O.

While there are similar trends in conversion, a clear difference in the product spectrum for the two catalysts exists. The Rh catalyst converts C_2H_6 primarily to syngas, with minor products being CO_2, H_2O, and C_2H_4. Platinum yields considerable quantities of C_2H_4 and comparable selectivity to H_2 and H_2O. At low C/O, CO is favored, while at high C/O, the temperature drops, and selectivity to CO decreases, thus a maximum is exhibited in the C_2H_4 selectivity. In both cases, equilibrium product distribution is not attained at all.

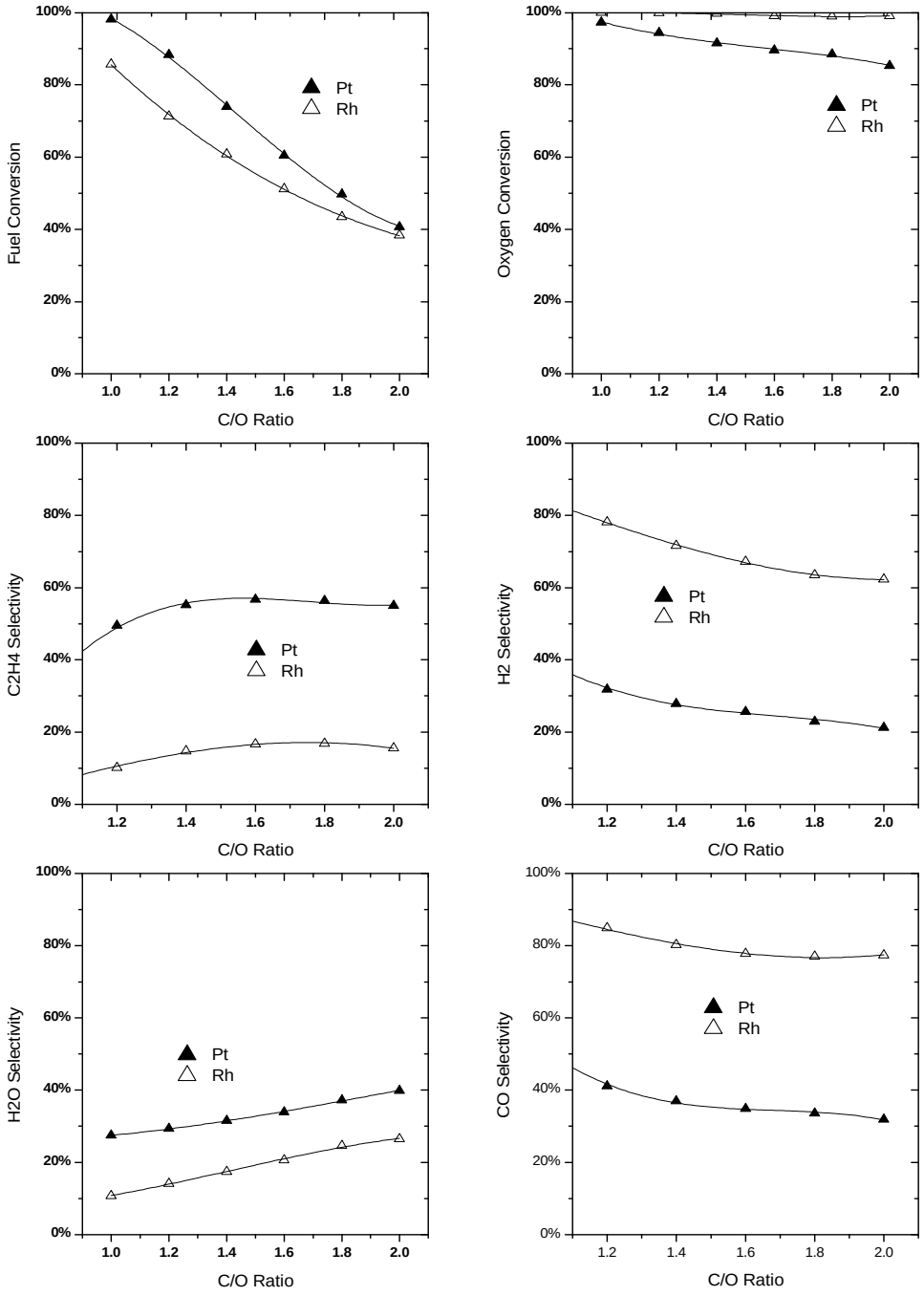

Figure 3- 2: Integral reactor performance in the ODH of C_2H_6 on Pt and Rh.

Results seen in Figure 3-2 are slightly different from those published elsewhere with undiluted feeds [11, 31, 33]. Part of the reason is due to the fact that air stoichiometry is mimicked in this work. While the inert moderates the reaction temperature, the average reaction rate is also lowered, hence lower conversions. The effect of dilution has been extensively tested elsewhere at is has been shown to be a sensitive parameter [11]. This work still employed air as an oxidizer, particularly because it is more favorable than having pure O_2 as a feed, which is quite expensive on large industrial scale.

To understand how the reactants progress to the products observed at the effluent, and what processes may dictate the differences between catalyst type and equilibrium, spatial reactor profiles of temperature and species flow were acquired for the same feeds as in Figure 3-2. The spatial profiles obtained at low C/O follow.

3.3.2 Spatially Resolved Measurements on Pt and Rh at Low C/O

To summarize C_2H_6, is capable of undergoing a myriad of reactions applicable to this work noted as follows:

Complete Combustion:	$C_2H_6 + \frac{7}{2}O_2 \rightarrow 2CO_2 + 3H_2O$	ΔH_f^o = - *1429 kJ/mol* *(R1)*
Partial Oxidation:	$C_2H_6 + O_2 \rightarrow 2CO + 3H_2$	ΔH_f^o = - *137 kJ/mol* *(R2)*
ODH :	$C_2H_6 + \frac{1}{2}O_2 \rightarrow C_2H_4 + H_2O$	ΔH_f^o = - *105 kJ/mol* *(R3)*
Steam Reforming (SR):	$C_2H_6 + 2H_2O \rightarrow 2CO + 5H_2$	ΔH_f^o = + *346 kJ/mol* *(R4)*
Dehydrogenation:	$C_2H_6 \rightarrow C_2H_4 + H_2$	ΔH_f^o = + *137 kJ/mol* *(R5)*

Figure 3-3 shows spatial profiles obtained during C_2H_6 ODH from C/O ratio of 1.2 for Pt and Rh. Axial position from -5 to 0 shows half of the FHS where no reactions are seen, from 0 to 10 is the catalytic region and thereafter represents the BHS. Profiles were taken in BHS to check for further homogenous chemistry, both oxidative and non-oxidative.

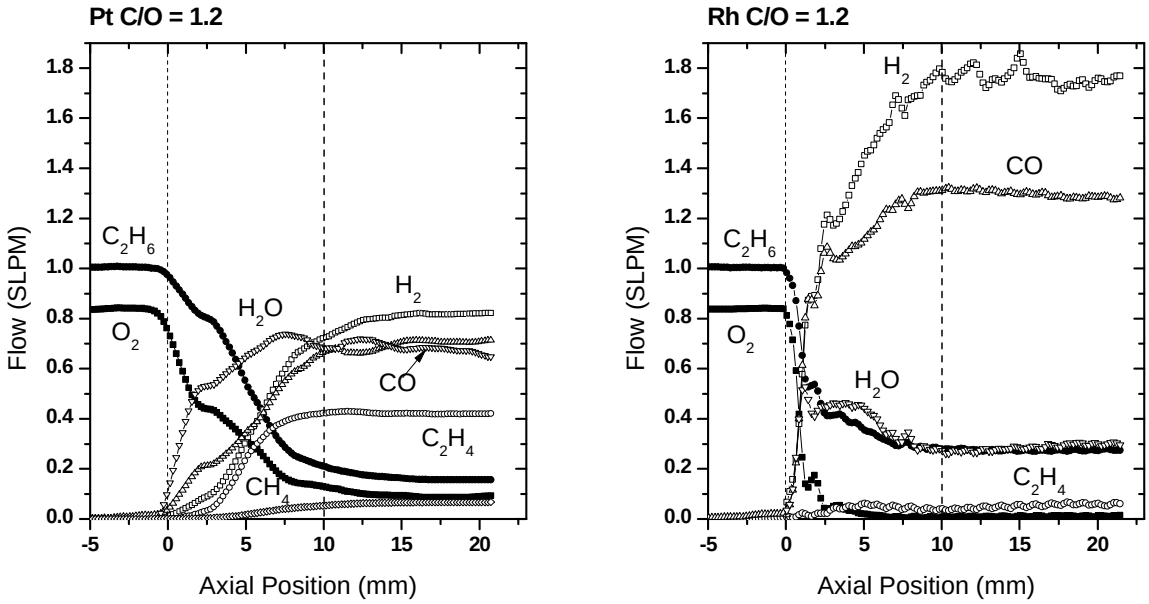

Figure 3- 3: Major species spatial profiles for Pt and Rh at C/O=1.2 during the ODH of C_2H_6. Not shown are minor products CO_2 and C_2H_2.

For the Pt catalyst, the major products in the first few millimeters are H_2O and CO, whereas the major products for Rh are H_2 and CO. In addition to the product spectrum, the rate of reaction is different for the two catalysts; Rh more rapidly consumes O_2 and > 99% is converted in the first ~3 mm whereas C_2H_6 and O_2 react slower over Pt with incomplete O_2 conversion throughout. On Rh, there is shift in the rate at which C_2H_6 is converted once most of the O_2 has been converted. Complete combustion and partial oxidation to syngas are quite dominant on Rh. Nonetheless, the relatively rapid reaction in the first parts of the two catalysts are exothermic, and appear to be largely responsible for the differences in CO, H_2, and H_2O species observed at the effluent. The steam reforming phenomena is observed on Rh, a process that occurs till the end of the catalytic section. As observed by Horn et al. [48], H_2O production was not produced 1:1 with C_2H_4. For this reason, those authors argued that C_2H_4 production did not occur as direct oxidative dehydrogenation (eq 3), but from pyrolysis of C_2H_6.

It should be noted that some bumps in the signals are largely due to irregularities in reticulated foam monoliths due to their manufacturing process. The result is a

macroporous structure consisting of cells, windows, struts, internal voids and microporosity which may channel gases differently depending on orientation. This presumably results in localized bypass and recirculation. As mentioned before, for this reason, the unique 3D structure and internal pore remnants from processing make the mechanical characterization and modeling of reticulated forms difficult [52]. As such, when taking spatial profiles, the sampling hole was placed in 90^o increments radially to compare and ensure that the profiles taken were representative of the foam independent of orientation.

In addition, data was obtained on numerous catalysts (5 for Pt and 4 for the Rh) to verify the independence of the chemistries seen between monoliths. While the axial species concentration differed very slightly in shape from monolith to monolith and different catalyst orientations, the average trends seen are reported here, with both checks being consistent within the limits of the study. The experimental data was slightly filtered and smoothed using the Savitsy-Golay technique [62], but the degree of filtering used is low enough to just clear noises from the QMS, thereby keeping the data raw with monolithic features showing. To see whether or not the same phenomena seen at the oxygen rich regime is present at fuel rich regimes, spatial profiles were taken at high C/O and are presented next.

3.3.3 Spatially Resolved Measurements on Pt and Rh at High C/O

The main features seen at low C/O are also depicted in this region. Pt still shows significant O_2 breakthrough while on Rh, it is converted rapidly producing syngas and H_2O. Ethane conversion is still much lower on Pt. With Pt, C_2H_4 formation at C/O = 2 occurs at a position further downstream than at C/O = 1.2, while the locus of ~50% O_2 conversion is roughly at the same position, suggesting that O_2 conversion before and after this point is dominated by different processes.

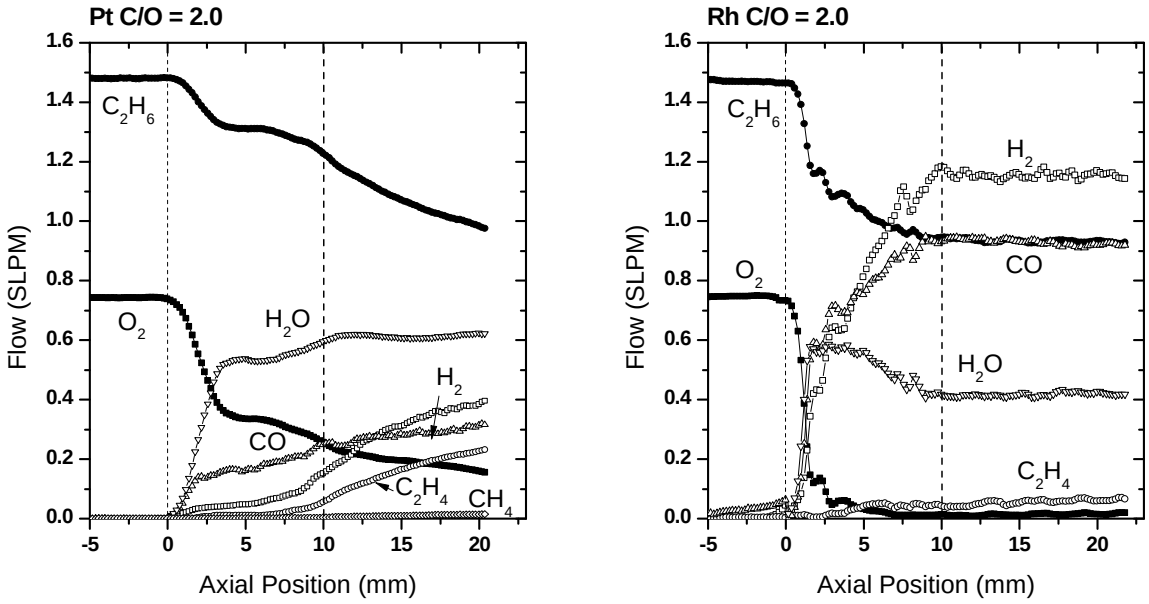

Figure 3- 4: Major species spatial profiles for Pt and Rh at C/O=2.0 during the ODH of C_2H_6. Not shown are minor products CO_2 and C_2H_2.

In addition to surface catalyzed routes, gas phase reactions to CO and H_2O may exist downstream. Although most of the O_2 is converted in the center monolith, nearly 50% of the overall C_2H_6 conversion takes place in the back heat shield, along with a substantial fraction of the C_2H_4 production. Oxidation of Pt can form bulk Pt_xO_y whose relative abundance depends on the oxidation temperature [63]. While these oxides should not be non volatile at high temperatures i.e. (> 600^{o}C) [63, 64] and at steady state, when preheating and cooling down the reactor, very small amounts of these oxides can migrate into the back heat shield. Its catalytic contribution to homogenous chemistry is therefore considered minimal.

In contrast, Rh distinctly shows two zones; the first is the oxidation zone that has a steeper slope (in terms of C_2H_6 and O_2 conversion) and the second slope change signifies the onset of steam reforming. The chemistry on Rh suggest that it is indeed mostly catalytic in nature, with no fuel conversion whatsoever after exiting the catalyst. Both catalysts seem to show two distinct zones but exhibit have very different product distribution, so drastic that the heat integration in the CPO reactor is thought to also play an important role.

3.3.4 Spatially Resolved Temperature Profiles

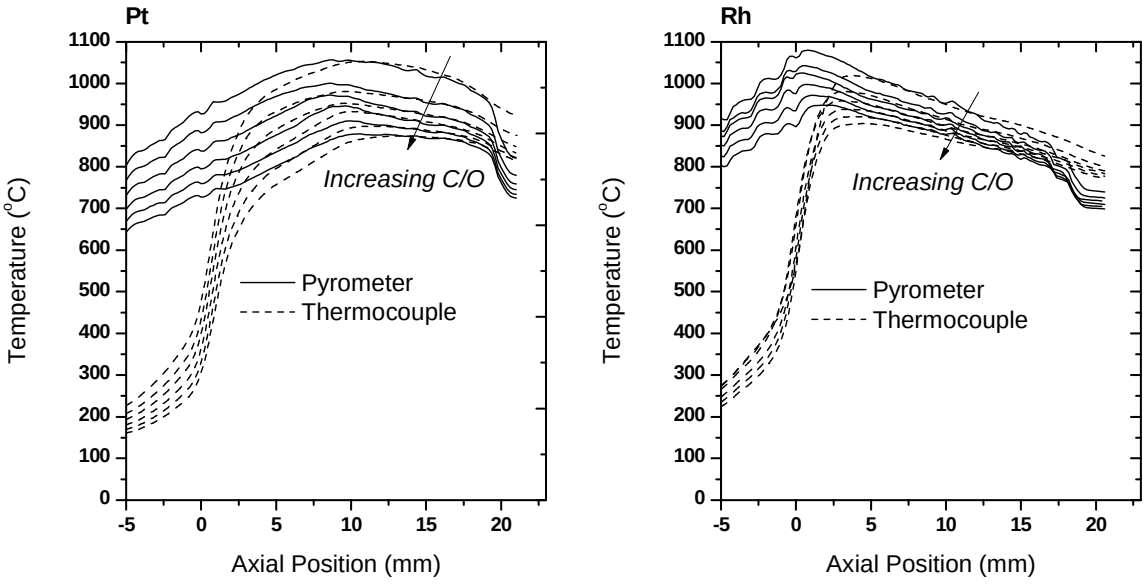

Figure 3- 5: Axial temperature profiles for C/O range of 1.0 to 2 in 0.2 increments.

As shown in Figure 3-5, the temperature profiles exhibited by both catalysts are quite different as inferred in the species profiles and integral data presented earlier. From the BHS up to about 2.5-3mm, Rh runs consistently hotter than Pt by as much as 100^{o}C. However shortly afterwards, there is a sharp temperature decline on Rh, consistent with the SR reaction (eqn R4), which is highly endothermic. This decline occurs on Pt at negligible gradients. At the end of the monolith, the highest temperature on Rh 910^{o}C at C/O =1.0, whereas for Pt, the lowest temperature exiting the monolith is at C/O = 2 at 920^{o}C. Pt therefore runs hotter that Rh for a larger portion of the monolith. Rh however, seems to show a consistent oxidation zone as seen by the similar thermocouple temperature rise in the first 3 mm of the monolith which is invariant of C/O.

It is important to note that the temperatures shown above are a good approximation of the gas phase (thermocouple) and catalyst surface (pyrometer) temperatures. The very low N_{Re}, coupled with the high length (of catalyst) to diameter (of pore) ratio (L/d_p) (which is approximately 20 for 45 ppi monoliths), suggests that axial dispersion is always low. Therefore heat transfer from the monolith to the gas occurs

primarily by conduction, a process that is limited to length in space and time. In this work, it is shown in Figure 3-5 that surface temperature measurements and gas temperature measurements are quite different at certain points; in the FHS (up to 550^{o}C), at the catalyst entrance (up to 450^{o}C). Not until ~3-4 mm (goes as far as 8mm for Pt) do gas and surface temperature match, indicating severe heat transfer limitations at the catalyst entrance.

Despite these limitations, foam monoliths are desired because of their high thermal conductivity, which leads to small radial temperature gradients, hence reducing the risk of hot spots and enabling a uniform catalytic activity. Radial temperature profiles taken by Flick and Huff showed that the temperature profile is flat across the monolith, with a slight drop where the catalyst joins the back heat shield [65]. Given the heat transfer limitations in the front face, it would be ideal to find a way to raise catalyst temperature in the front face without consuming feed ethane. This notion is explored with H_2 addition profiles shown next, as done in previous works [11, 33].

3.3.5 Effect of H_2 Addition

The effect of H_2 addition was explored only at the optimal ethylene production point (C/O=2). Equimolar amounts of H_2 and C_2H_6 were added, a reaction that can be quite explosive. These mixtures are flammable while stationary, but the flow rate through the reactor is high enough that the velocity through the premixed portion of the reactor is high enough and exceeds the homogenous flame speed [65].

Based on the hydrogen addition results below, it becomes clear that the catalyst does indeed play a key role in the ODH of ethane. Here, preferential oxidation of hydrogen to produce H_2O occurs up to 3.5 mm on Pt and 1 mm on Rh. The scheme is sequential as follows:

$$H_2 + \frac{1}{2}O_2 \rightarrow H_2O \qquad \Delta H^{o} = -241.8 \text{ kJ/mol} \qquad (3.7)$$

$$C_2H_6 \rightarrow C_2H_4 + H_2 \qquad \Delta H^{o} = +136.8 \text{ kJ/mol} \qquad (3.8)$$

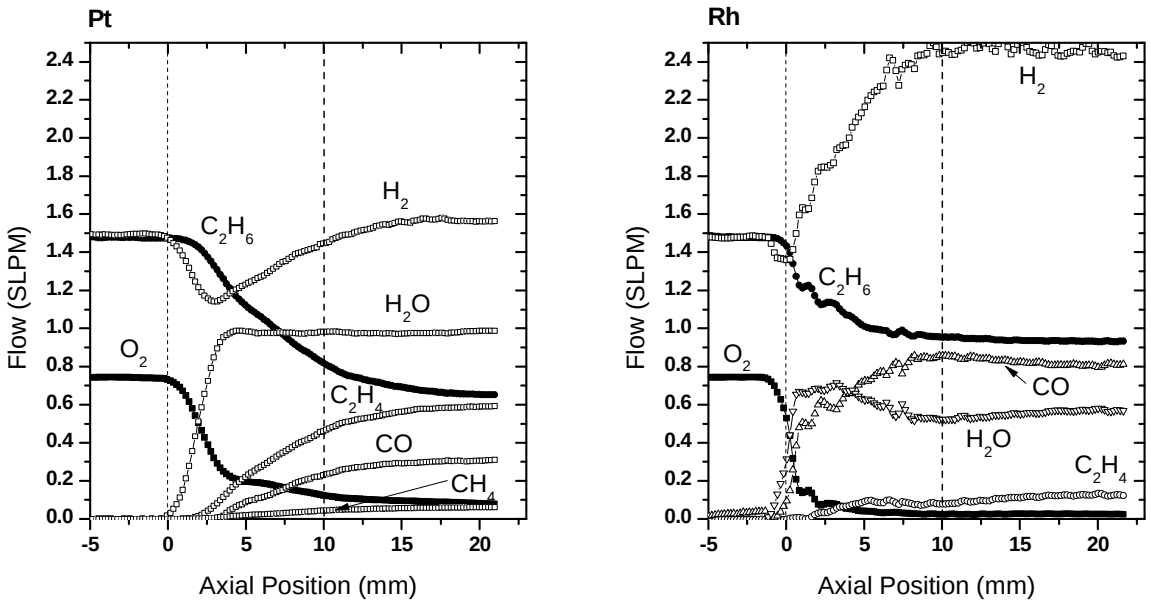

Figure 3- 6: H_2 addition spatial profiles for Pt and Rh in the ODH of C_2H_6.

	Pt		Rh	
$C_2H_6/O_2/H_2$	2/1/0	2/1/2	2/1/0	2/1/2
Conversion (%)				
C_2H_6	41	57	38	40
O_2	85	93	99	98
Selectivity (%)				
CO	32	18	77	62
CO_2	11	1	7	3
CH_4	2	4	0	2
C_2H_4	55	77	16	33
T_{max}, °C				
Pyrometer	879	970	946	952
Thermocouple	875	946	902	920

Table 3- 2: Comparison of effluent reactor performances for Pt and Rh with and without H_2 addition.

Preferential oxidation of H_2 is sufficient enough to raise the catalyst temperature, allowing for homogeneous reaction ignition possibly when H_2 consumption ceases. At this point, homogenous and heterogeneous reactions begin, even on Rh were a very small amount of ethylene was produced in the absence of H_2 addition. Heterogeneously produced CO formation is lower than at C/O=2, particularly due to the delay in C_2H_6 conversion. Diffusion theory supports preferential oxidation of H_2 because the flux of H_2 is ≈ 4 times that of C_2H_6, for it is an inverse function of the molecular weight [10]. For either catalyst, the addition of H_2 improves the selectivity to C_2H_4 at the effluent, as indicated in Table 3-2, however, the spatial profiles show much more pronounced effect for the Pt catalyst in comparison to the profile without H_2 addition.

Water is the primary product in the first few mm, which further indicates a preferential oxidation of H_2. Further downstream, C_2H_6 consumption begins to form CO, C_2H_4, and H_2 along with minor amounts of CO_2, CH_4 and H_2O. The consumption of C_2H_6 begins prior to complete conversion of H_2. However, a distinct minimum can be observed in the H_2 profile, clearly partitioning the reactor. Production of H_2 and C_2H_4 in the second zone occur at approximately 1:1, and slow to their final values by the end of the catalyst. Temperature profiles obtained are shown next.

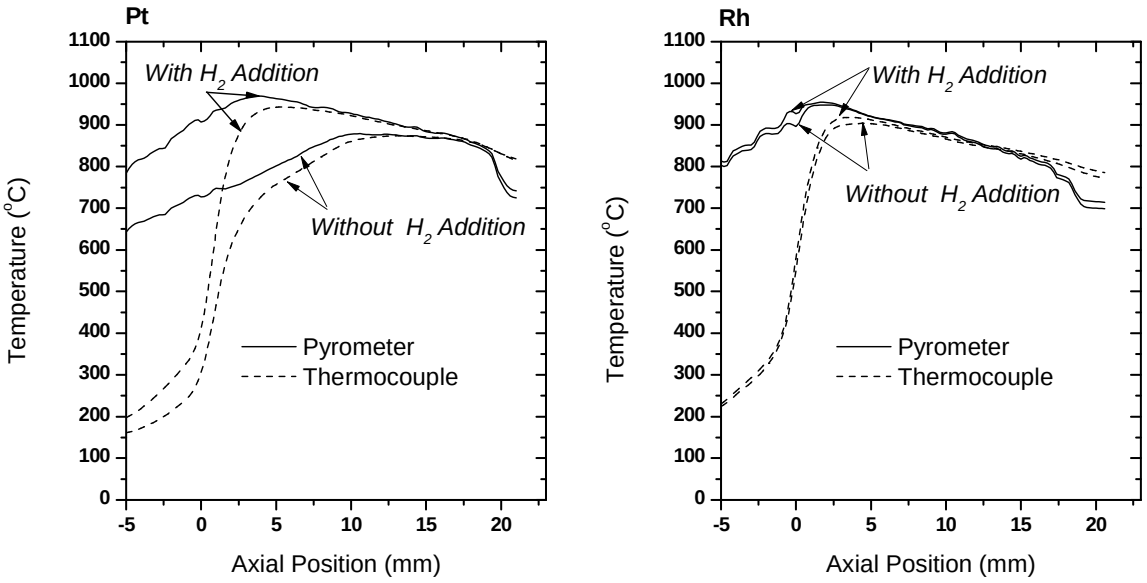

Figure 3- 7: Reactor temperature profiles, measured by pyrometer (solid lines) and thermocouple (dashed lines) for C/O = 2, with and without H_2 addition.

Consistent with the temperature profiles, reactions on Rh display similar behavior to the case without co-feed with the exception of the H_2 curve, which is translated upward by approximately the amount fed. A subtle minimum can be observed in the H_2 flow near the entrance of the catalyst; however, it is too small to discern whether or not it occurs in the absence of C_2H_6 consumption with certainty. A maximum is present in the H_2O curve, indicating the presence of downstream steam reforming. In work done by Hickman and Schmidt on methane CPO, the difference in H_2 selectivity was explained by the higher activation energy for OH formation on Rh (84 kJ/mol), compared to Pt (11 kJ/mol) [13, 66]. Therefore on Rh, H atoms are more likely to combine and desorb as H_2 than on Pt (OH formation on Rh is unstable as shown by laser induced fluorescence (LIF) [67]) which allows faster formation of OH species, resulting in more H_2O production. Clearly from the temperature profiles, it is evident that H_2 addition raised the catalyst temperature further upstream allowing homogeneous ignition earlier into the monolith. This phenomenon is readily seen on Pt.

3.4 Discussion[1]

In this work, Pt and Rh were compared, and a number of differences and similarities can be observed in the product and temperature evolutions. The profiles are similar in the respect that (1) exothermic reactions occur rapidly very near the entrance of the catalyst leading to CO, CO_2, H_2, and H_2O, (2) the average catalyst temperatures are high enough for C_2H_6 pyrolysis, (3) low C_2H_2 selectivities are observed, and (4) coke accumulation was not observed. The profiles are different in the respect that (1) O_2 is completely consumed in the first few mm of the Rh catalyst while it remains throughout the Pt catalyst, (2) steam reforming dominates the downstream section of the Rh catalyst while it is apparently absent on Pt, (3) temperature increases sharply over Rh while more slowly over Pt, except with mixtures with H_2 addition.

[1] Parts adapted from Brian C. Michael, David N. Nare, and Lanny D. Schmidt "Catalytic partial oxidation of ethane to ethylene and syngas over Rh and Pt coated monoliths: spatial profiles of temperature and composition." *In Submission to CES*

In experiments done by Sasaki et al on Rh and Pt foils using the molecular beam technique, C_2H_6 oxidation reactions proceeded to temperatures above 930^oC and the only products detected were CO, H_2 and H_2O. Based on the reaction order measurements over Pt, it was noted that activated C_2H_6 reacted with O_2 to produce ethoxy species, precursors for hydrogen production [68]. While the production rates on Rh were much smaller, lower O_2 partial pressure was required to produce CO and H_2, a phenomenon directly related to a higher O_2 affinity of Rh. In agreement with this conclusion, the higher oxygen coverage on Rh resulted in a lower experimental oxygen breakthrough.

However, Rh was unselective to C_2H_4 production, hence the discussion in the next few paragraphs will focus on Pt. Determining the contributions of pure homogeneous versus pure heterogeneous contributions is tricky, particularly because oxygen is always present. Under the presence of oxygen, ethyl radicals are more readily formed via an oxidative pyrolysis step than via thermal degradation [69]. Respectively, they occur as follows:

$$C_2H_6 + OH\bullet \rightarrow C_2H_5\bullet + H_2O \quad (3.9)$$

$$C_2H_6 \rightarrow C_2H_5\bullet + H\bullet \quad (3.10)$$

Zerkel et al evaluated both reactions and concluded that reaction 3.9 is much faster than reaction 3.10 at the high solid temperatures experienced in ODH [39]. From TPR studies, it is known that C_2H_6 reactions in the absence of a catalyst do not occur until ≈ 650^oC [70]. Therefore, in the temperatures employed in these tests, radical pools should have been formed. However, minimal or no ethylene productions is seen in the 1-2 mm of the catalyst, where TPR reactions predict its formation in the absence of a catalyst. This indicates that the catalyst is playing a role where competitive reactions occur. Vincent et al argued that the rapid consumption of oxygen at the entrance of the catalyst and high selectivity to water is the principal surface reaction mechanism. Spatially resolved measurements do show this phenomenon. Based on the argument of preferential H_2 oxidation [42], and the lower activation for energy for OH formation , the major catalytic reaction paths on Pt suggested by Vincent et al are:

$$H_s + O_s \rightleftharpoons OH_s + Pt_s \quad (3.11)$$

$$H_s + OH_s \rightleftharpoons H_2O_s + Pt_s \quad (3.12)$$

From spatially resolved measurements, large production of CO and H_2 is observed at the catalyst entrance. For H_2 production, Vincent et al proposed the following dominant catalytic reaction, consistent with conclusions from LIF studies [67].

$$H_s + H_s \rightleftharpoons H_2 + 2Pt_s \quad (3.13)$$

Regarding CO production on Pt, its formation is quite complex, and has been a subject of study for numerous groups [71-74]. Many mechanisms can occur as follows:

$$C_s + O_s \rightleftharpoons CO + 4Pt_s \quad (3.14)$$

$$C_s + O_s \rightleftharpoons CO + 2Pt_s \quad (3.15)$$

$$C_s + OH_s \rightleftharpoons CO + H_s + 3Pt_s \quad (3.16)$$

$$C_s + OH_s \rightleftharpoons CO + H_s + Pt_s \quad (3.17)$$

Vincent et al's work, whose experimental and theoretical results are mirrored the most, concluded that the last two reactions (eqn 3.16 and 3.17) are dominant. There is a sharp temperature increase in this region, following which homogeneous reactions ignite, resulting in an onset of C_2H_4 formation. This region on Pt is seen when the slope of H_2O formation changes. Water formation at this point can be presumed to be mostly by the oxidative pyrolysis reaction 3.9. Regarding CO_2 formation, Heracleous et al argued that it is produced from CO overoxidation, a phenomenon that was not seen during homogenous oxidation reactions, concluding that this reaction is surface assisted and can be attributed exclusively to the presence of the catalytic material [70]. Therefore, following the onset of homogeneous reactions, all schemes proceed as a combination of heterogeneous and homogeneous routes, including cracking to ethylene.

Many other studies agree with this finding, stating that homogenous reactions indeed play a fundamental role in the high temperature production of olefins, even for millisecond residence time scales. From TPR studies, ethylene was thought to be produced by primarily a dehydrogenation mechanism, even in the presence of oxygen in

the gas phase [70]. Surface pathways were therefore thought to have a significant role, even at temperatures where homogenous reactions occurred, indicating the possible occurrence of homogenous-heterogeneous reaction scheme.

In the ODH of C_2H_6 over Pt/Al_2O_3, experiments were performed at high temperatures and short contact times under both isothermal and adiabatic conditions, with comparison to predictions of detailed kinetic models on homogeneous oxidative pyrolysis. After a comparison of the catalytic data with gas phase experiments, the bulk data suggested that the production of ethylene could be largely explained by single contribution of radial reactions [75]. In simulations done by Zerkle et al, it was suggested that platinum-catalyzed heterogenous chemical processes and are responsible for the oxidation of surface carbon and hydrogen, resulting in localized heat in to the gas phase as suggested similarly by experiments in [38, 40, 75].

3.5 Conclusions on ODH of C_2H_6 on Pt and Rh

Product evolution in the ethane ODH of C_2H_6 at high resolution was obtained using spatially resolved measurements. Experiments and analysis done on Pt suggested that C_2H_6 was undergoing combustion and partial oxidation reactions. But their quantitative contributions were contrasting and incongruent. As such, insight was sought from a well-known combustion, oxidation and reforming catalyst Rh. The results show C_2H_6 being capable of undergoing reactions inferred.

Further analysis of the experimental data at all stoichiometries studied showed behavior on Pt and Rh suggestive of catalytic reactions. High H_2 production on Rh was explained by the higher activation energy for OH formation on Rh compared to Pt. Rh exhibited a low oxygen breakthrough, a phenomenon directly related to a higher O_2 affinity on Rh than Pt. The temperature profiles on Pt confirmed its poor reforming ability, allowing for excellent ethylene yields. Pt therefore is a good ethylene catalyst because its oxidation ability is near that of Rh, but reforming reactions are much slower, hence homogeneously produced ethylene is not reformed away and it maintains a higher temperature throughout the reactor.

A definite correlation can be made between C_2H_4 production and reactor temperature, namely that regardless of C/O the temperature required for C_2H_4 production over Pt is >750 ºC, which agrees with other reports of the onset of homogeneous reactions. Surface pathways were therefore thought to have a significant role, even at temperatures where homogenous reactions occurred, indicating the possible occurrence of a homogenous-heterogeneous reaction scheme. To check for these effects, hydrogen addition to ethane ODH was examined. Spatial profiles indeed confirmed preferential oxidation of H_2 that provided the heat required to drive endothermic steam cracking, resulting in higher ethylene selectivity.

The reactor system was thought to be largely under mass transfer limitation, while heat transfer from the catalyst to the bulk gases was thought to be poor in the first few mm of the catalytic section. A two-zone model is thus confirmed, with accurate representation on species evolution; on Pt, heterogeneous oxidation of ethane to syngas and H_2O followed by onset of homogeneous chemistry, specifically dehydrogenation reactions. On Rh, the same oxidation chemistry occurs followed by endothermic reforming of ethane to syngas. The importance of spatial profiles is therefore unparalleled, clearly showing product evolution and temperature data, parameters highly valuable in accurately modeling CPO reactors and ethane ODH.

Chapter 4

Effect of Sn and Cu Addition to Pt during ODH

4.1 Summary

In this chapter, the motivation to study bimetallic catalysts is first presented, giving insight into their robustness and industrial applications. Following which the integral results obtained on Pt-Sn and Pt-Cu are compared to those of Pt. Noting that effluent data on the bimetallic catalysts show differences in product distribution with Pt, (with bimetallics showing higher ethylene selectivity), species profiles are sought. Spatial profiles at both low and high C/O are shown and discussed. Spatially resolved temperature profiles are given next, focusing on gas phase temperatures. The effect of H_2 addition to bimetallic catalysts is explored. Conclusions on Pt in comparison to Pt-Sn and Pt-Cu performances are then drawn.

4.2 Motivation for Bimetallics Study[2]

Bimetallic catalysts containing Pt as the main constituent followed by a second metal such as Ir, Sn, Re or Cu on alumina are commonly used in reforming reactions in industry [76] since the discovery of the platforming processes in the late 1940's. The role platforming process play involves reforming molecules in low octane naphtha to produce a high octane gasoline component by addition of a second metal to Pt. Some examples of industrial bimetallic catalyst applications are the Pt-Au combination for emissions control [77], the Pt-Cu system for dechlorination of chlorinated hydrocarbons [78] and the Pd-Au catalyst for the production of vinyl acetate [79].

Noble metals such as Pt and Au are generally expensive; hence preparation of highly dispersed catalysts is desirable to maximize the surface area of the active metals. It has been proposed that addition of a second metal causes a geometric effect, diluting Pt atoms thereby decreasing the average ensemble size [80, 81]. Additional theories also suggest that there is a change in bond strength between chemisorbed hydrocarbons and Pt surface atoms due to electron transfer from the promoter to Pt known as the electronic effect [82]. Compared to Pt alone, bimetallic catalysts have shown to be more stable, more selective and convert hydrocarbons with higher activity [83]. As such, some studies on bimetallic catalysts have sought to obtain information about metal dispersion and surface composition in an effort to gain knowledge about the catalytic roles of each component [84].

One particular hydrocarbon system that has been studied on both mono [11] and bimetallic [33] catalysts is the oxidative dehydrogenation (ODH) of ethane to produce ethylene. Ethylene is a very important industrial compound particularly because of its high reactivity and versatility, which it owes from having a double bond. It is

[2] Parts adapted from David N. Nare and Lanny.D. Schmidt "Effect of Cu and Sn addition to Pt in the authothermal oxidative dehydrogenation of ethane at short contact time: spatially resolved measurements." *In preparation*

conventionally produced via steam cracking, a process that is highly endothermic, therefore energy intensive.

In this chapter, the focus is on comparing Pt to Pt-Sn and Pt-Cu catalysts which have shown to give high yields to ethylene. To test for geometric effects and to decipher the existence of these metals on the catalyst surface and gain insight as to how they affect product distribution, some characterization is done. Moreover, species and temperature profiles which show the products evolve in the catalyst bed in bimetallic systems of this nature are captured and shown for the first time. The objective is to show the effect of Sn and Cu addition on the spatial variation of important reactions and products as well as temperature.

Note: The catalyst preparation for bimetallic catalysts was different from monometallics. Please refer back to catalyst preparation, reduction and conditioning in section 2.4 for a details.

4.3 Results

4.3.1 Integral Reactor Performance

Figure 4-1 (next) shows the integral results on the ODH of ethane on 45 ppi Pt, Pt-Sn and Pt-Cu foam monoliths. For bimetallic catalysts, only 2% Pt/ 2% metal was used because it has been shown that Pt performance is invariant of metal loading for metal loading >1% [85]. The effect of adding a second metal was the point of interest. The results show that C_2H_6 conversion decreases monotonically on all metals with increasing C/O ratio due to the dilution effect as the feed becomes O_2 lean. Pt-Sn is superior in converting feed ethane from 98% to 50% with increasing C/O than both Pt-Cu (97% to 47%) and Pt (98% to 41%). In contrast, O_2 conversion is significantly lower on both bimetallics than on Pt alone, averaging 8-10% less. The presence of O_2 can therefore be thought to play a major role as both Pt-Sn and Pt-Cu are highly selective to desired C_2H_4, maximizing at 64% compared to Pt at 50%. Again, comparison of selectivities is done based on C or H selectivity as defined in the definitions section.

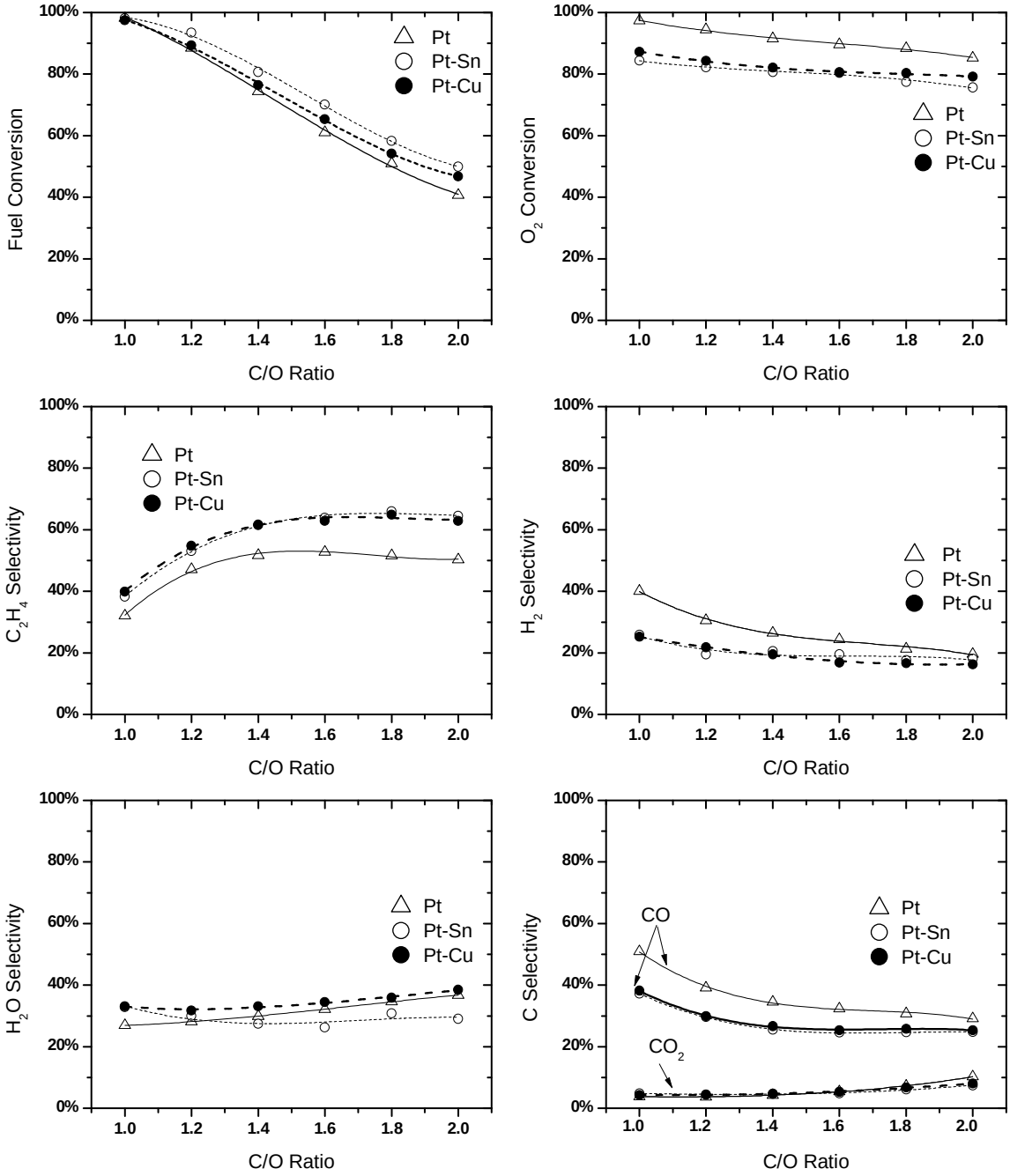

Figure 4- 1: Integral data for C_2H_6 ODH on Pt, Pt-Sn and Pt-Cu.

Because the bimetallic catalysts exhibit higher C_2H_6 conversion and selectivity to the desired product, C_2H_4 yields are also higher on Pt-Sn and Pt-Cu. Also shown in Figure 4-1 is that both Pt-Sn and Pt-Cu produce significantly less amounts of CO which

is desirable in industrial applications, particularly because CO is known to poison noble metal catalysts. H_2 selectivity is higher on Pt but approaches that of bimetallics as C/O increases, while Pt-Sn and Pt-Cu remain around the same level. Even though the work done by Yokoyama et al was at constant 30% N_2 dilution, the trends seen in the results are qualitatively comparable.

The integral data suggests that there exists competing chemistries resulting in olefin, syngas or combustion products formation. Adiabatic thermodynamic product distribution is not attained according to calculations performed in HSC [59]. High levels of syngas, and not ethylene, are predicted by equilibrium with complete conversion of C_2H_6 at all stoichiometries. Solid carbon formation is expected with increasing C/O, but under experimental conditions studied, negligible carbon formation was observed (i.e. no reactor shutdown after > 60 hours of operation). However analyzing just the reactor effluent is not sufficient in validating modeling efforts. Consequently, as stated earlier, the objective of this work is to capture species evolution and transport phenomena axially during the ODH of ethane on mono and bimetallic catalysts. The spatial profiles obtained follow.

4.3.2 Spatially Resolved Measurements on Pt, Pt-Sn and Pt-Cu at Low C/O

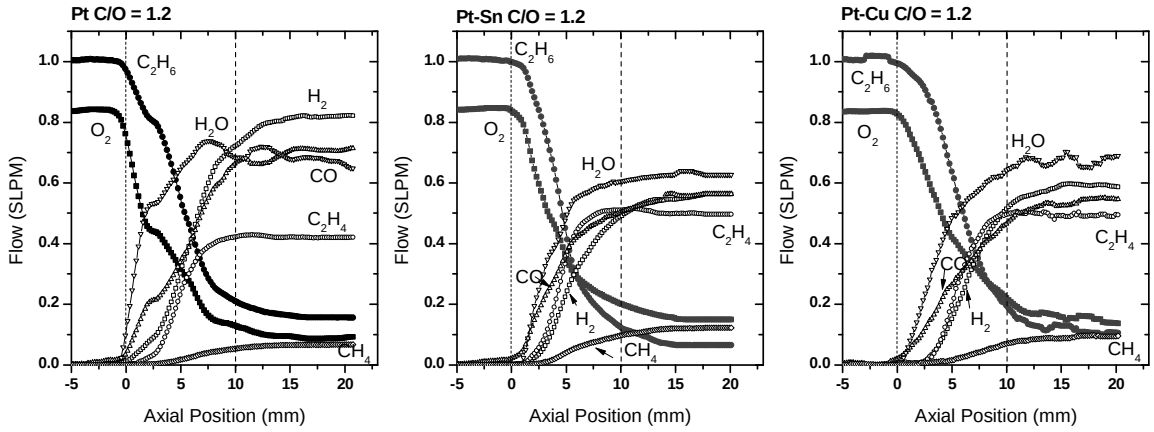

Figure 4- 2: Major species spatial profiles for 2% metal loading at low C/O for (R) Pt (C) Pt-Sn (L) Pt-Cu. Not shown are minor CO_2 and C_2H_2.

In the profiles shown in Figure 4-2, contributions from the above C_2H_6 is capable of undergoing as summarized in equations R1-R7 in section 3.3.2 are evident. In the first few mm of the catalyst, H_2O is always produced first followed by CO. Not shown in the profiles are minor products CO_2 and C_2H_2 which account for less than 5% of the C and H balances. Large production of syngas and H_2O indicate that combustion chemistry is dominant in the first few mm of the catalyst where both C_2H_6 and O_2 are rapidly converted. Combustion chemistry is exothermic and must raise the catalyst temperature to a point where production of C_2H_4 begins, located around the 1-2.5 mm mark for all catalysts. Pt produces the most H_2O and H_2 whereas Pt-Sn and Pt-Cu produce the most C_2H_4 and a lower amount of CO. To see whether or not the same phenomena seen at the oxygen rich regime is present at fuel rich regimes, spatial profiles were taken at high C/O and are presented next.

4.3.3 Spatially Resolved Measurements on Pt, Pt-Sn and Pt-Cu at High C/O

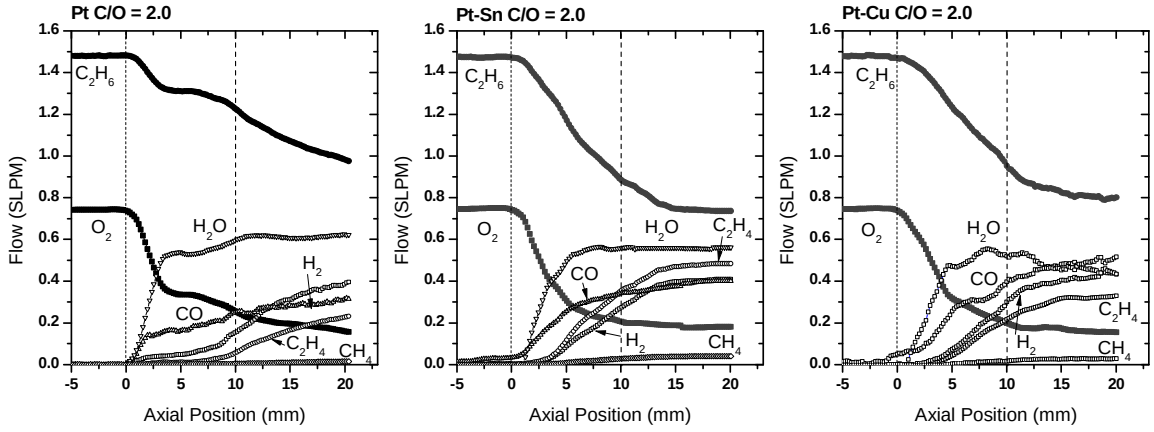

Figure 4- 3: Major species spatial profiles for 2% metal loading at high C/O for (R) Pt (C) Pt-Sn (L) Pt-Cu. Not shown are minor CO_2 and C_2H_2.

As seen in the integral results shown previously, the highest selectivity to C_2H_4 occurred at C/O ratio of 2.0 for bimetallics, while Pt levels off around C/O = 1.6, coincident with the ODH reaction stoichiometry (eqn R3). The spatial profiles obtained are shown in Figure 4-3 above. Unlike at low C/O, the dilution effect of more fuel lowers

the temperature thereby slowing all reactions. Fuel and oxygen conversion is much lower for all catalysts but more so for Pt. On Pt, almost 50% of the total fuel converted occurs in the BHS, indicating that there exists a significant amount of homogeneous chemistry. Production of C_2H_4 occurs 7.5 mm downstream for Pt, whereas it at 2.5 mm for both Pt-Sn and Pt-Cu. For all catalyst, the rate of formation for H_2 and C_2H_4 is almost equal, indicating that the dehydrogenation reaction (eqn R5) is the most dominant. Gas phase partial oxidation must also play a role since there is some CO production downstream.

The drastic differences between the monometallic and the bimetallic systems stem primarily in the catalytic region which naturally extends downstream. Chemistry on the bimetallics is much faster, converting >83% of the overall C_2H_6 conversion inside the catalyst region. Hydrogen production on Pt-Sn and Pt-Cu now exceeds that of Pt seen at low C/O even though the selectivities are the same as shown in Figure 4-3. But this is because of the definition of selectivity (in which the denominator is converted fuel).

In addition, while CH_4 production is small, it is more pronounced on the bimetallics than on Pt. On the other hand, Pt still produces the largest amount of H_2O and shows similar O_2 breakthrough seen with the bimetallics. While species concentrations along the reactor give insight into chemistries occurring and the rates at which they occur, heat balances taken accurately in situ have been missing in the literature but may help elucidate some of these differences. Temperature profiles taken for all reaction conditions tested (except H_2 addition which will be presented later) are shown next.

4.3.4 Spatially Resolved Temperature Profiles

Figure 4-4 (next) shows temperature profiles obtained for Pt, Pt-Sn and Pt-Cu. In these profiles, only thermocouple data is shown particularly because the points of interest to allow for comparison lie in gas phase temperatures. Moreover, this work has shown that CPO reactors are heat transfer limited in the front face; catalyst surface and gas temperatures equilibrate at some point inside the monolith. Hence gas phase temperatures allows for a more realistic comparison. It can be noted that Pt is always

hotter at the catalyst entrance than both Pt and Pt-Sn at all stoichiometries. However, inside the monolith through to the exit, both bimetallics exceed Pt alone. At C/O =1.0, the maximum temperatures attained are 1052^{o}C, 1130^{o}C and 1110 ^{o}C for Pt, Pt-Sn and Pt-Cu respectively. Similary for C/O =2.0, the maximum temperatures attained in the same order are 873^{o}C, 923^{o}C and 898^{o}C. Clearly the bimetallics run hotter, essentially leading to faster reaction rates as seen in the catalytic conversion of C_2H_6 and O_2. Supporting the faster rates is that Pt-Sn and Pt-Cu have steeper gradients (temperature rise) from the catalyst entrance to about 5mm in the axial direction. The temperatures in the BHS are sufficiently high to allow for homogeneous chemistry seen in spatial profiles presented before.

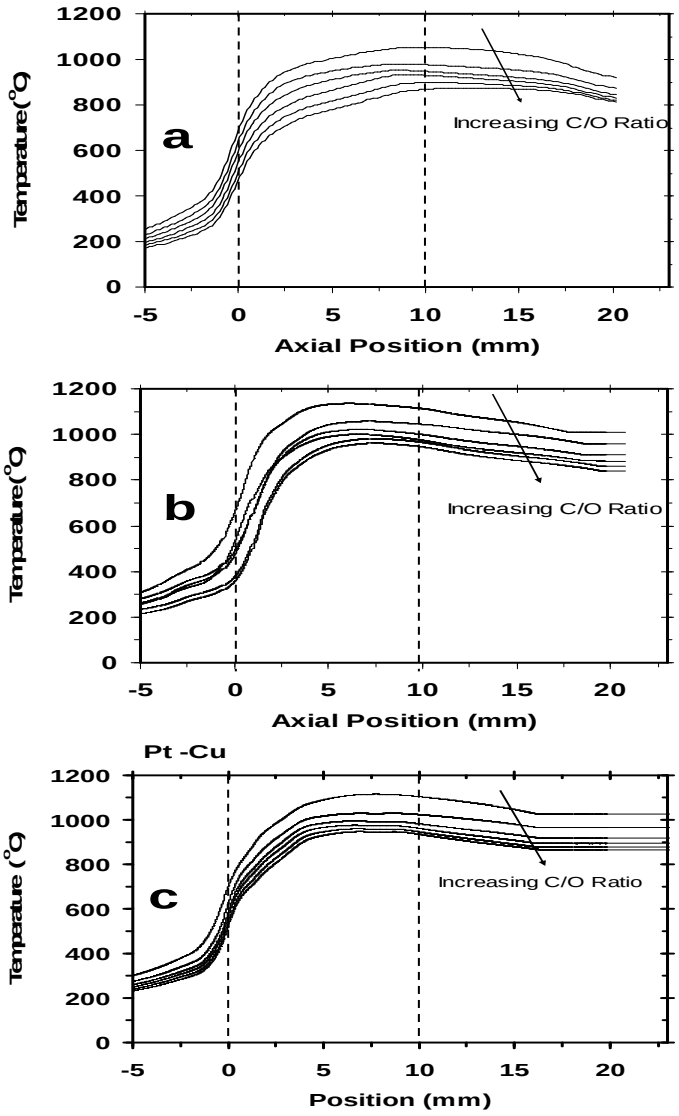

Figure 4- 4: Axial temperature profiles for C/O range of 1.0 to 2 in 0.2 increments for (a) Pt (b) Pt-Sn and (c) Pt-Cu. Measurements done using a thermocouple.

4.3.5 Effect of H_2 Addition

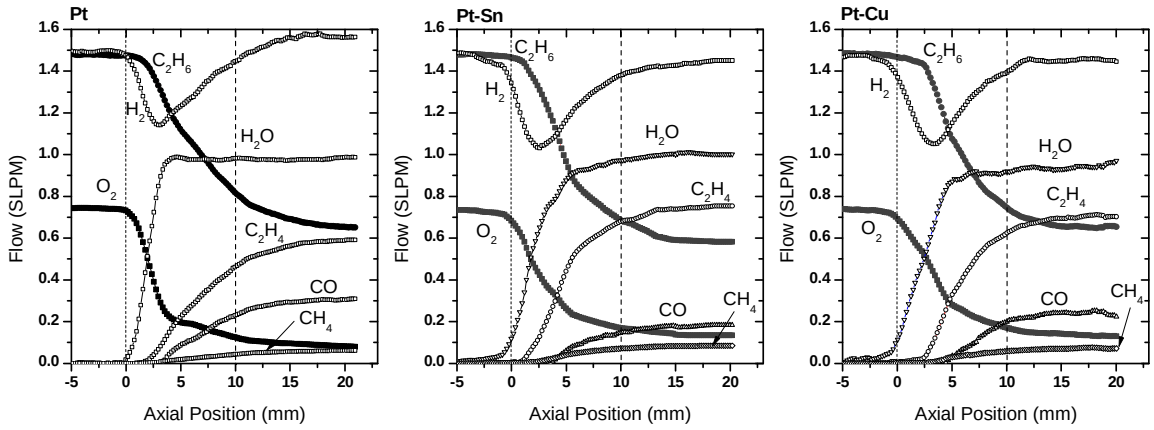

Figure 4- 5: H_2 addition spatial profiles for (R) Pt (C) Pt-Sn and (L) Pt-Cu.

	Pt		Pt-Sn		Pt-Cu	
$C_2H_6/O_2/H_2$	2/1/0	2/1/2	2/1/0	2/1/2	2/1/0	2/1/2
Conversion (%)						
C_2H_6	41	57	50	60	47	56
O_2	85	93	76	82	79	84
Selectivity (%)						
CO	32	18	25	7	25	9
CO_2	11	1	8	1	8	1
CH_4	2	4	3	5	2	4
C_2H_4	55	77	65	85	63	85
T_{max}, ºC						
Thermocouple	879	970	961	964	946	962

Table 4- 1: Comparison of effluent reactor performances for Pt, Pt-Sn and Pt-Cu with and without H_2 addition

Based on the hydrogen addition results shown in Figure 4-5, it becomes clear that the catalyst does indeed play a key role in the ODH of C_2H_6. In the first few mm, there is

preferential oxidation of H_2 to produce large amounts of H_2O, an occurrence seen on all catalysts. Up to 30% of feed H_2 is consumed on Pt-Sn which shows to be the best H_2 oxidizer than both Pt and Pt-Cu. Pt-Cu is very similar to Pt-Sn is terms of deep oxidation of H_2 but goes slightly deeper into the monolith. Temperature profiles taken and shown in Figure 4-6 agree with this assertion, where the temperature rise on Pt (light grey) rises then maximizes at the same level as Pt-Sn but it is moved further downstream. The scheme is still largely interpreted to sequential, allowing for a two zone model which begins with preferential oxidation of H_2, forming H_2O followed by dehydrogenation of C_2H_6 to C_2H_4 and H_2.

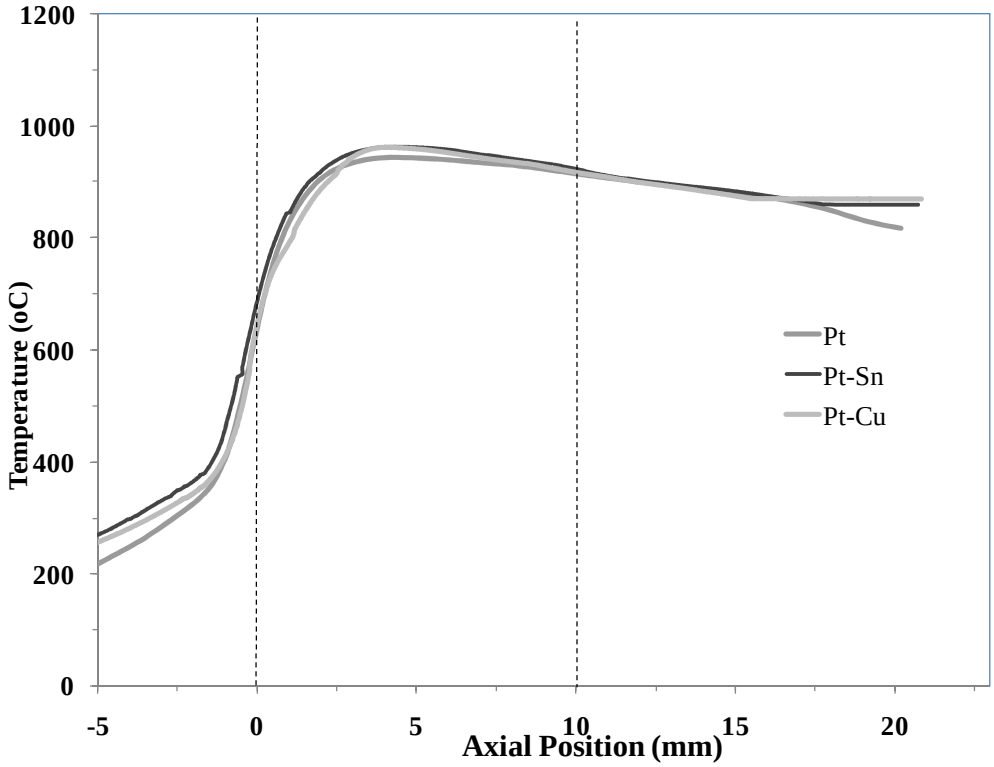

Figure 4- 6: H_2 Addition temperature profiles for Pt, Pt-Sn and Pt-Cu measured using a thermocouple.

Due to its exothermic nature, preferential oxidation of H_2 is sufficient enough to raise the catalyst temperature, allowing for homogeneous reaction ignition possibly when H_2 consumption ceases. When C_2H_6 conversion begins at the end of zone 1, there is onset

of C_2H_4 formation, where the C_2H_4/H_2 production ratio is approximately unity. Simple dehydrogenation reactions are too slow however to produce the large amounts of C_2H_4 observed. In addition, there still exist heterogeneously produced CO (whose formation is significantly suppressed on the bimetallics) compared to Pt and CO_2 (not shown). Therefore, in agreement with arguments made by Schmidt et al, an assertion can be made that the catalyst surface generates active species that increase the rate of gas phase reactions [86]. Hence at this point, homogenous and heterogeneous reactions are coupled and occur simultaneously. High selectivity to ethylene is achieved once H_2 is added at C/O=2 where on Pt, it rises from 55% to 77%, on Pt-Sn from 65% to 85% and on Pt-Cu from 63% to 85%. The large ethylene production occurs because of the delay in oxidative consumption of ethane.

4.4 Conclusions on ODH of C_2H_6 on Pt, Pt-Sn and Pt-Cu

In the spatial profiles taken, Pt-Cu and Pt-Sn seem to show comparable performances in many ways. The temperature profiles follow a similar trend, with Pt-Sn running approximately 20-30^oC hotter at any given axial location. While Pt temperatures are sufficient to allow for homogenous pyrolysis ignition of ethane (700^oC), production of C_2H_4 occurs further into the monolith with increase in C/O. On the contrary, bimetallic catalysts show C_2H_4 production almost instantly, particularly because the temperatures would have exceeded 750^oC at the catalytic entrance.

Ethane conversion occurs faster on bimetallic catalysts than on Pt, and so does O_2 conversion. At the effluent, Pt-Sn and Pt-Cu have larger C_2H_6 conversions that Pt, hence CO formation is significantly lower on bimetallic catalysts. Also noted is than Pt-Sn produced more C_2H_2 than all catalysts, even though its selectivity is still small. Pt-Sn and Pt-Cu showed that they are superior to Pt in terms of deep oxidation of H_2. While the temperature profiles were within close ranges, Pt-Sn and Pt-Cu also converted C_2H_6 better than Pt alone, hence high selectivity to C_2H_4 was obtained. The results showed that selectivity to C_2H_4 rose once H_2 is added. In all cases, the large amounts of C_2H_4 production occur because of the delay in oxidative consumption of C_2H_6.

Preliminary SEM images taken (not shown) suggest that geometric effects do indeed exist. Particles on the bimetallic catalysts were more dispersed and smaller in average size, essentially decreasing their ensemble sizes. This is desirable because more catalyst surface area becomes available if highly dispersed. Contributions due to chemical effects are hard to decipher at this point. XPS and EDS data to be taken in the near future should help answer this question. Thus far, the major differences noted, making bimetallic catalysts superior, are as follows; better oxidation ability hence faster conversion of C_2H_6 resulting in attainment of homogenous ignition temperatures earlier into the monolith and better deep oxidation of H_2. All catalyst show equal poor reforming ability, an attribute desirable in sustaining reactor temperatures, thereby obtaining high selectivity to C_2H_4.

Chapter 5

Thesis Summary and Future Directions

5.1 Summary

This chapter begins by summarizing the research done as part of this thesis. After which details regarding future directions are given. First is a discussion on the need to perform extensive characterization to help elucidate on chemical and geometric effects more fully. Spatially resolved transients are also proposed, information that can be used to obtain empirical rates and minimize start up times. The carbon burn off experiment using the spatial technique is also proposed. To correctly classify the evolution of product H_2 versus that unconverted from the feed, isotope D_2 addition is proposed. Finally experiments using lower PPI monoliths and well as at elevated pressures are proposed as a way to aid homogenous chemistry.

5.2 Thesis Summary

In this work, a technique of spatially resolved measurements, devised recently in the Schmidt group, is put to test in the oxidative dehydrogenation of ethane to ethylene. A CPO reactor is used. The advantages of using this kind of a reactor is that the process is autothermal, negligible carbon formation is noted experimentally and minimal emission of green house gases is attained.

Tests on monometallic catalysts were done on Pt and Rh. Pt proved to be an excellent oxidation catalyst, as such maintained high temperatures throughout the reactor. Rh was an even better oxidation catalyst than Pt, converting feed ethane quickly in the first few mm. It also showed a consistent oxidation zone, after which endothermic steam reforming reactions of ethane started once >99% of feed oxygen was converted. These steam reforming reactions resulted in a steep temperature decline inside the reactor. The effect of hydrogen addition showed a two zone reactor model; first preferential oxidation of hydrogen to water followed by homogeneous pyrolysis of ethane to ethylene. Rh was essentially unselective to hydrogen oxidation, a phenomenon attributed to the higher activation energy for hydroxyl formation.

Motivated by previous studies and patents, the effect of Sn and Cu addition to Pt making a robust bimetallic catalyst was also studied. A different catalyst preparation and conditioning technique was used. Spatially resolved measurements showed that bimetallic catalysts had a shorter oxidation zone that Pt, converted ethane faster, had higher selectivities to ethylene and suppressed CO_x formation. When hydrogen addition experiments were performed, both Pt-Sn and Pt-Cu were better at deep oxidation of hydrogen. This, along with faster ethylene conversion, gave maximum selectivity to ethylene at 85% even though temperature profiles were very similar.

Preliminary work to test the geometric effects show that Pt-Sn and Pt-Cu exhibit higher dispersed particles and smaller ensembles. More work remains to be done in this area to fully elucidate the chemical effects. In conclusion, spatial concentration and species profiles were taken for the first time during ODH of C_2H_6. The results are promising in optimization and supporting modeling efforts.

5.3 Future Directions

The findings obtained in this work can be suggestive of new research and additional research areas to further understand CPO and/or ODH reactions at industrially relevant conditions.

5.3.1 Catalyst Characterization

Species and temperature profiles are quite insightful in detailing how products evolve along the catalyst. Heat and mass balances provide valuable information to aid modeling efforts. However to fully distinguish between chemical and geometric effects, characterization of catalysts may prove helpful. The chemical state of the noble metals before and after the reaction, the nature of the bimetallics and whether or not they form alloys or intermetallic compounds and if they migrate at all once exposed to high temperatures still remains to be known. Specifically, data from fresh and used catalysts obtained from scanning transmission electroscopy (TEM), energy dispersive spectroscopy (EDS), x-ray diffraction (XRD) and x-ray photoelectronic spectroscopy (XPS) will help elucidate and give insights into what catalytic properties are needed to further optimize ethylene production.

5.3.2 Spatially Resolved Transients

Spatially resolved measurements can be used to obtain transient data at select positions inside the monoliths channel, following which kinetic parameters can be obtained. In these experiments, the C/O ratio can be varied in a stepwise manner from say C/O=1 to C/O=2 or intermediate points by changing the fuel and keeping Ar and O_2 constant. The Ar flow can also be adjusted stepwise to reflect constant space velocity to allow for direct comparison.

In other cases, the C/O ratio can be changed by switching all flows from one extreme end another. Information that can be obtained from transient experiments like this include, classification of mass transport limitations, confirmation as to whether heating up to or cooling down from the optimal ethylene production point affects the rate of ethylene formation and how much time it takes to produce the desired product once a C/O is changed. The apparent activation energies for C_2H_4 formation can be derived from Arrhenius plots, similar to work done by Horn et al on CPO of methane on Rh [87].

This experimental effort can be combined with numerical simulations to predict transient reactor behavior, thereby avoiding overshoots and undershoots in the catalyst and reactor temperature. One can also minimize start-up times as shown in work done by Williams et al on methane transient product analysis [88]. For ethane ODH, transient data can be taken on a new catalyst at a specified C/O to figure out when steady state production of ethylene is achieved.

5.3.3 Deuterium Addition

In this work, it has been shown that H_2 addition results in preferential oxidation of hydrogen in the first section of the two-zone model proposed. However the evolvement of hydrogen and how much of it is produced cannot be differentiated from unreacted H_2 or that from dehydrogenation and oxidation reactions. As such, isotopic substitution using deuterium can be used instead of H_2. D_2 will still be preferentially oxidized, followed by dehydrogenation as follows:

$$D_2 + \frac{1}{2}O_2 \rightarrow D_2O \qquad \Delta H^o = -\ 249\ \text{kJ / mol} \qquad (5.1)$$

$$C_2H_6 \rightarrow C_2H_4 + H_2 \qquad \Delta H^o = +\ 136.8\ \text{kJ/mol} \qquad (5.2)$$

Using the QMS, the origin of the H_2 produced can be accurately accounted for. D_2 would shown up as m/z = 4 whereas H_2 would show as m/z = 2.

5.3.4 Elevated Pressure Measurements

It is important to consider what transport processes are dominant in the monolithic studies provided. The tortuosity and randomness of the foam structure determines how fluid flows in the reactor. The bulk gas is well mixed and high axial velocities render axial species diffusion negligible compared with convection. It has been shown that in the CPO of methane, O_2 consumption is determined by mass transport and a given conversion was reached at the same axial coordinate regardless of C/O [89]. A somewhat similar phenomenon was observed here with Pt and Rh.

Radial dispersion however cannot be neglected, especially for reactions that show a large contribution of homogeneous activity as seen in spatial profiles. The overall performance of the catalyst at experimental ranges explored can therefore be explained by maximum selectivities attained. In theory, too small of pore sizes translate into abundance of heterogeneous chemistry and reforms the ethylene produced away, while too large pores cannot allow enough oxidation chemistry to occur so as to produce the heat needed for homogeneous ethylene production. In experiments done on 45-80 ppi foams, 45 ppi foams gave the best performance to ethylene [90], but very minor differences were seen in agreement with [85]. In other studies, flow rate in ODH was varied by a factor of 50 and the conversion and selectivity remained the same, whereas oxygen conversion was always complete [91]. It can be inferred that the dehydrogenation of ethylene becomes rate limiting after complete oxygen conversion.

But for academic purposes, it would be beneficial to try 30 PPI foams to see if homogenous chemistry is aided. With ethane dehydrogenation, higher yields are expected at elevated pressures, hence experiments beyond atmospheric pressures provide for a good future direction.

Bibliography

1. Smalley, R.E. *The Top Ten Problems of Humanity for Next 50 Years*. in *Energy & NanoTechnology Conference*. 2003. Rice University.
2. CIA. 2008 [cited; Available from: https://www.cia.gov/library/publications/the-world-factbook/.
3. Chen, J.Q., et al., *Recent advancements in ethylene and propylene production using the UOP/Hydro MTO process.* Catalysis Today, 2005. **106**(1-4): p. 103-107.
4. Ren, T., M. Patel, and K. Blok, *Olefins from conventional and heavy feedstocks: Energy use in steam cracking and alternative processes.* Energy, 2006. **31**(4): p. 425-451.
5. Albright, L.F., B.L. Crynes, and W.H. Corcaran, *Pyrolysis: Theory and Industrial Practice."* 1983, New York: Academic Press.
6. Nakamura, D., *Special report: Ethylene capacity rising, margins continue to suffer.* Oil and Gas, 2002: p. 68.
7. Kniel, L., O. Winter, and K. Stork, *Ethylene: Keystone to the petrochemical industry*. 1980, New York: Marcel Dekker, Inc.
8. Schmidt, L.D., *The Engineering of Chemical Reactions*. 1998, New York: Oxford University Press.
9. DOE, *Manufacturing Consumption Energy Survey*. 1998, Energy Information Administration of the US Department of Energy: Washington DC.
10. Geankoplis, C.J., *Transport Processes and Seperation Process Principles*. 4th ed. 2003, Upper Saddle River, NJ: Pearson Education. Inc.
11. Bodke, A.S., et al., *Oxidative Dehydrogenation of Ethane at Millisecond Contact Times: Effect of H_2 Addition.* Journal of Catalysis, 2000. **191**(1): p. 62-74.
12. IPCC, *The third assessment report: climate change – mitigation*. 2001, International Panel on Climate Change: Geneva.
13. Hickman, D.A. and L.D. Schmidt, *Production of Syngas by Direct Catalytic Oxidation of Methane.* Science, 1993. **259**(5093): p. 343-346.
14. Dreyer, B.J., et al., *Autothermal steam reforming of higher hydrocarbons: n-Decane, n-hexadecane, and JP-8.* Applied Catalysis A: General, 2006. **307**(2): p. 184-194.
15. Salge, J.R., et al., *Renewable Hydrogen from Nonvolatile Fuels by Reactive Flash Volatilization.* Science, 2006. **314**(5800): p. 801-804.
16. Subramanian, R., et al., *Catalytic partial oxidation of higher hydrocarbons: reactivities and selectivities of mixtures.* Chemical Engineering Science, 2004. **59**(22-23): p. 5501-5507.
17. Krummenacher, J.J., K.N. West, and L.D. Schmidt, *Catalytic partial oxidation of higher hydrocarbons at millisecond contact times: decane, hexadecane, and diesel fuel.* Journal of Catalysis, 2003. **215**(2): p. 332-343.
18. Williams, K.A. and L.D. Schmidt, *Catalytic autoignition of higher alkane partial oxidation on Rh-coated foams.* Applied Catalysis A: General, 2006. **299**: p. 30-45.
19. Deluga, G.A., et al., *Renewable Hydrogen from Ethanol by Autothermal Reforming.* Science, 2004. **303**(5660): p. 993-997.

20. Colby, J.L., P.J. Dauenhauer, and L.D. Schmidt, *Millisecond autothermal steam reforming of cellulose for synthetic biofuels by reactive flash volatilization.* Green Chemistry, 2008. **10**(7): p. 773-783.
21. Iordanoglou, D.I. and L.D. Schmidt, *Oxygenate Formation from n-Butane Oxidation at Short Contact Times: Different Gauze Sizes and Multiple Steady States.* Journal of Catalysis, 1998. **176**(2): p. 503-512.
22. Song, X., L.D. Schmidt, and R. Aris, *Steady states and oscillations in homogeneous--heterogeneous reaction systems.* Chemical Engineering Science, 1991. **46**(5-6): p. 1203-1215.
23. Wanat, E.C., B. Suman, and L.D. Schmidt, *Partial oxidation of alcohols to produce hydrogen and chemicals in millisecond-contact time reactors.* Journal of Catalysis, 2005. **235**(1): p. 18-27.
24. Matsuda, T., et al., *Dehydrogenation of isobutane to isobutene in a palladium membrane reactor.* Applied Catalysis A: General, 1993. **96**(1): p. 3-13.
25. Liebmann, L.S. and L.D. Schmidt, *Oxidative dehydrogenation of isobutane at short contact times.* Applied Catalysis A: General, 1999. **179**(1-2): p. 93-106.
26. Bharadwaj, S.S. and L.D. Schmidt, *Olefins by Catalytic Oxidation of Alkanes in Fluidized-Bed Reactors.* Journal of Catalysis, 1995. **155**(2): p. 403-413.
27. Krummenacher, J.J. and L.D. Schmidt, *High yields of olefins and hydrogen from decane in short contact time reactors: rhodium versus platinum.* Journal of Catalysis, 2004. **222**(2): p. 429-438.
28. Le Bars, J., et al., *Role of surface acidity on vanadia/silica catalysts used in the oxidative dehydrogenation of ethane.* Applied Catalysis A: General, 1992. **88**(2): p. 179-195.
29. Erdöhelyi, A. and F. Solymosi, *Oxidation of ethane over silica-supported alkali metal vanadate catalysts.* Journal of Catalysis, 1991. **129**(2): p. 497-510.
30. Huff, M., P.M. Torniainen, and L.D. Schmidt, *Partial oxidation of CH_4, C_2H_6, and C_3H_8 on monoliths at short contact times.* Natural Gas Conversion II, 1993(July 4-9).
31. Huff, M. and L.D. Schmidt, *Ethylene formation by oxidative dehydrogenation of ethane over monoliths at very short contact times.* The Journal of Physical Chemistry, 1993. **97**(45): p. 11815-11822.
32. Yokoyama, C., S.S. Bharadwaj, and L.D. Schmidt, *Platinum-tin and platinum-copper catalysts for autothermal oxidative dehydrogenation of ethane to ethylene.* Catalysis Letters, 1996. **38**(3): p. 181-188.
33. Bodke, A.S., et al., *High Selectivities to Ethylene by Partial Oxidation of Ethane.* Science, 1999. **285**(5428): p. 712-715.
34. Huff, M.C. and L.D. Schmidt, *Elementary step model of ethane oxidative dehydrogenation on Pt-coated monoliths.* AIChE Journal, 1996. **42**(12): p. 3484-3497.
35. D. A. Hickman, L.D.S., *Steps in CH_4 oxidation on Pt and Rh surfaces: High-temperature reactor simulations.* AIChE Journal, 1993. **39**(7): p. 1164-1177.
36. Ranzi, E., et al., *Lumping procedures in detailed kinetic modeling of gasification, pyrolysis, partial oxidation and combustion of hydrocarbon mixtures.* Progress in Energy and Combustion Science, 2001. **27**(1): p. 99-139.

37. Silberova, B., et al., *Low-temperature oxidation reactions of ethane over a Pt/Al_2O_3 catalyst.* Journal of Catalysis, 2003. **219**(1): p. 206-213.
38. Beretta, A., E. Ranzi, and P. Forzatti, *Oxidative dehydrogenation of light paraffins in novel short contact time reactors. Experimental and theoretical investigation.* Chemical Engineering Science, 2001. **56**(3): p. 779-787.
39. Zerkle, D.K., et al., *Understanding Homogeneous and Heterogeneous Contributions to the Platinum-Catalyzed Partial Oxidation of Ethane in a Short-Contact-Time Reactor*. Journal of Catalysis, 2000. **196**(1): p. 18-39.
40. Beretta, A. and P. Forzatti, *High-Temperature and Short-Contact-Time Oxidative Dehydrogenation of Ethane in the Presence of Pt/Al_2O_3 and $BaMnAl_{11}O_{19}$ Catalysts.* Journal of Catalysis, 2001. **200**(1): p. 45-58.
41. Huff, M.C., et al., *The Contribution of Gas-Phase Reactions in the Pt-Catalyzed Conversion of Ethane-Oxygen Mixtures.* Journal of Catalysis, 2000. **191**(1): p. 46-54.
42. Vincent, R.S., et al., *The chemistry of ethane dehydrogenation over a supported platinum catalyst.* Journal of Catalysis, 2008. **260**(1): p. 37-64.
43. York, A.P.E., T. Xiao, and M.L.H. Green, *Brief Overview of the Partial Oxidation of Methane to Synthesis Gas.* Topics in Catalysis, 2003. **22**(3): p. 345-358.
44. Marengo, S., P. Comotti, and G. Galli, *New insight into the role of gas phase reactions in the partial oxidation of butane.* Catalysis Today, 2003. **81**(2): p. 205-213.
45. Basini, L., et al., *Catalytic partial oxidation of natural gas at elevated pressure and low residence time.* Catalysis Today, 2001. **64**(1-2): p. 9-20.
46. Basile, F., et al., *Partial oxidation of methane: Effect of reaction parameters and catalyst composition on the thermal profile and heat distribution.* Catalysis Today, 2001. **64**(1-2): p. 21-30.
47. A. Henning, D. and L. D. Schmidt, *Oxidative dehydrogenation of ethane at short contact times: species and temperature profiles within and after the catalyst.* Chemical Engineering Science, 2002. **57**(14): p. 2615-2625.
48. Horn, R., et al., *Spatial and temporal profiles in millisecond partial oxidation processes.* Catalysis Letters, 2006. **110**(3): p. 169-178.
49. Twigg, M.V. and J.T. Richardson, *Theory and Applications of Ceramic Foam Catalysts.* Chemical Engineering Research and Design, 2002. **80**(2): p. 183-189.
50. Smith, R.T., R.M. Sambrook, and J.G.P. Binner, *Novel processing of foam ceramics.* Materials Research Society Symposium - Proceedings, 1995. **371**: p. 279-284.
51. Gibson, L.J. and M.F. Ashby, *Cellular Solids, Structures and Properties*. 1988, Oxford, UK: Pergamon Press.
52. Strom, L.A., et al., *Novel applications of fully sintered reticulated ceramics.* Materials Research Society Symposium - Proceedings, 1995. **371**: p. 321-326.
53. Richardson, J.T., Y. Peng, and D. Remue, *Properties of ceramic foam catalyst supports: pressure drop.* Applied Catalysis A: General, 2000. **204**(1): p. 19-32.
54. Moulijn, J.A. and F. Kapteijn, *Potential of monolithic reactors in catalysis; multiphase applications.* Materials Research Society Symposium - Proceedings, 1999. **549**: p. 3-8.

55. Litovsky, T., et al., *Thermal conductivity of high temperature ceramic thermal insulations.* Materials Research Society Symposium - Proceedings, 1995: p. 309-314.
56. Peng, Y. and J.T. Richardson, *Properties of ceramic foam catalyst supports: one-dimensional and two-dimensional heat transfer correlations.* Applied Catalysis A: General, 2004. **266**(2): p. 235-244.
57. Richardson, J.T., D. Remue, and J.K. Hung, *Properties of ceramic foam catalyst supports: mass and heat transfer.* Applied Catalysis A: General, 2003. **250**(2): p. 319-329.
58. Chin, Y.-H., et al., *Methanol steam reforming over Pd/ZnO: Catalyst preparation and pretreatment studies.* Fuel Processing Technology, 2003. **83**(1-3): p. 193-201.
59. HSC. [cited; Available from: http://www.hsc-chemistry.net/index.html.
60. Tester, J.W. and M. Modell, *Thermodynamics and Its Applications*. 1997: Prentice Hall.
61. Bartholomew, C.H., *Carbon Deposition in Steam Reforming and Methanation.* Catalysis Reviews, 1982. **24**(1): p. 67 - 112.
62. F.Chau, et al., *Chemometrics : From Basics to Wavelet Transform*. Chemical Analysis: A Series of Monographs on Analytical Chemistry and Its Applications, ed. J.D. Wineforduer. 2004: Wiley - Interscience.
63. Hwang, C.P. and C.T. Yeh, *Platinum-oxide species formed by oxidation of platinum crystallites supported on alumina.* Journal of Molecular Catalysis. A, Chemical, 1996. **112**(2): p. 295-302.
64. Yokoyama, C., S.S. Bharadwaj, and L.D. Schmidt, *Catalytic oxidative dehydrogenation process and catalyst*. 2000: United States Patent. p. 1-14.
65. Flick, D.W. and M.C. Huff, *Acetylene formation during the catalytic oxidative dehydrogenation of ethane over Pt-coated monoliths at short contact times.* Catalysis Letters, 1997. **47**(2): p. 91-97.
66. Hickman, D.A., E.A. Haupfear, and L.D. Schmidt, *Synthesis gas formation by direct oxidation of methane over Rh monoliths.* Catalysis Letters, 1993. **17**(3): p. 223-237.
67. Zum Mallen, M.P., W.R. Williams, and L.D. Schmidt, *Steps in H_2 oxidation on Rh: OH desorption at high temperatures.* Journal of physical chemistry(1952), 1993. **97**(3): p. 625-632.
68. Sasaki, T., et al., *Comparative study between methane and ethane in catalytic partial oxidation over Pt and Rh foils using molecular-beam technique.* Applied Catalysis A, General, 2007. **328**(2): p. 140-149.
69. Donsi, F., R. Pirone, and G. Russo, *Oxidative Dehydrogenation of Ethane over a Perovskite-Based Monolithic Reactor.* Journal of Catalysis, 2002. **209**(1): p. 51-61.
70. Heracleous, E. and A.A. Lemonidou, *Homogeneous and heterogeneous pathways of ethane oxidative and non-oxidative dehydrogenation studied by temperature-programmed reaction.* Applied Catalysis A, General, 2004. **269**(1-2): p. 123-135.
71. Alavi, A., et al., *CO Oxidation on Pt (111): An Ab Initio Density Functional Theory Study.* Physical Review Letters, 1998. **80**(16): p. 3650-3653.

72. Ebbesen, S.D., B.L. Mojet, and L. Lefferts, *In situ ATR-IR study of CO adsorption and oxidation over Pt/Al_2O_3 in gas and aqueous phase: Promotion effects by water and pH.* Journal of Catalysis, 2007. **246**(1): p. 66-73.
73. Krischer, K., M. Eiswirth, and G. Ertl, *Oscillatory CO oxidation on Pt(110): Modeling of temporal self-organization.* The Journal of Chemical Physics, 1992. **96**(12): p. 9161-9172.
74. Su, X., et al., *High-Pressure CO Oxidation on Pt(111) Monitored with Infrared-Visible Sum Frequency Generation (SFG).* Journal of the American Chemical Society, 1997. **119**(17): p. 3994-4000.
75. Beretta, A., E. Ranzi, and P. Forzatti, *Production of olefins via oxidative dehydrogenation of light paraffins at short contact times.* Catalysis Today, 2001. **64**(1-2): p. 103-111.
76. Balakrishnan, K. and J. Schwank, *A chemisorption and XPS study of bimetallic $Pt-Sn/Al_2O_3$ catalysts.* Journal of Catalysis, 1991. **127**(1): p. 287-306.
77. Nicolau, I., P.M. Colling, and L.R. Johnson, *Vinyl acetate catalyst preparation method*. 1994, Google Patents.
78. Harley, A.D., et al., *Processes for converting chlorinated byproducts and waste products to useful materials*. 1995, Google Patents.
79. Nakatsuji, T., *European Patent 0 602 602 A1*. 1993.
80. Cortright, R.D. and J.A. Dumesic, *Microcalorimetric, Spectroscopic, and Kinetic Studies of Silica-Supported Pt and Pt/Sn Catalysts for Isobutane Dehydrogenation.* Journal of Catalysis, 1994. **148**(2): p. 771-778.
81. Dautzenberg, F.M., et al., *Conversion of n-hexane over monofunctional supported and unsupported Pt-Sn catalysts.* J. Catal, 1980. **63**(1).
82. Verbeek, H. and W.H.M. Sachtler, *The study of the alloys of platinum and tin by chemisorption.* The Journal of Catalysis, 1976. **42**: p. 257-267.
83. Passos, F.B., D.A.G. Aranda, and M. Schmal, *Characterization and Catalytic Activity of Bimetallic $Pt-In/Al_2O_3$and $Pt-Sn/Al_2O_3$Catalysts.* Journal of Catalysis, 1998. **178**(2): p. 478-488.
84. Kim, M.H., et al., *Determination of metal dispersion and surface composition in supported Cu–Pt catalysts.* Journal of Catalysis, 2002. **208**(2): p. 381-392.
85. Bodke, A.S., S.S. Bharadwaj, and L.D. Schmidt, *The Effect of Ceramic Supports on Partial Oxidation of Hydrocarbons over Noble Metal Coated Monoliths.* Journal of Catalysis, 1998. **179**(1): p. 138-149.
86. Schmidt, L.D., J. Siddall, and M. Bearden, *New ways to make old chemicals.* AIChE Journal, 2000. **46**(8): p. 1492-1495.
87. Horn, R., et al., *Mechanism of H_2 and CO formation in the catalytic partial oxidation of CH_4 on Rh probed by steady-state spatial profiles and spatially resolved transients.* Chemical Engineering Science, 2007. **62**(5): p. 1298-1307.
88. Williams, K.A., C.A. Leclerc, and L.D. Schmidt, *Rapid lightoff of syngas production from methane: A transient product analysis.* AIChE Journal, 2005. **51**(1).
89. Horn, R., et al., *Methane catalytic partial oxidation on autothermal Rh and Pt foam catalysts: Oxidation and reforming zones, transport effects, and approach to thermodynamic equilibrium.* Journal of Catalysis, 2007. **249**(2): p. 380-393.

90. Donsì, F., et al., *The effect of support morphology on the reaction of oxidative dehydrogenation of ethane to ethylene at short contact times.* Catalysis Today, 2005. **105**(3-4): p. 551-559.
91. Witt, P.M. and L.D. Schmidt, *Effect of Flow Rate on the Partial Oxidation of Methane and Ethane.* Journal of Catalysis, 1996. **163**(2): p. 465-475.